

**OPTIC DISK DETECTION AND SEGMENTATION
APPROACHES BASED ON VESSEL NETWORK**

BY

NITTAYA MUANGNAK

**A DISSERTATION SUBMITTED IN PARTIAL FULFILLMENT OF
THE REQUIREMENTS FOR THE DEGREE OF DOCTOR OF
PHILOSOPHY (TECHNOLOGY)
SIRINDHORN INTERNATIONAL INSTITUTE OF TECHNOLOGY
THAMMASAT UNIVERSITY
ACADEMIC YEAR 2016**

**OPTIC DISK DETECTION AND SEGMENTATION
APPROACHES BASED ON VESSEL NETWORK**

BY

NITTAYA MUANGNAK

**A DISSERTATION SUBMITTED IN PARTIAL FULFILLMENT OF
THE REQUIREMENTS FOR THE DEGREE OF DOCTOR OF
PHILOSOPHY (TECHNOLOGY)
SIRINDHORN INTERNATIONAL INSTITUTE OF TECH
THAMMASAT UNIVERSITY
ACADEMIC YEAR 2016**



OPTIC DISK DETECTION AND SEGMENTATION APPROACHES BASED ON
VESSEL NETWORK

A Dissertation Presented

By

NITTAYA MUANGNAK

Submitted to

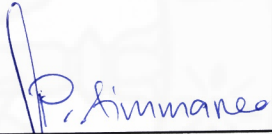
Sirindhorn International Institute of Technology

Thammasat University

In partial fulfillment of the requirements for the degree of
DOCTOR OF PHILOSOPHY (TECHNOLOGY)

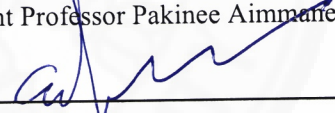
Approved as to style and content by

Advisor and Chairperson of
Thesis Committee



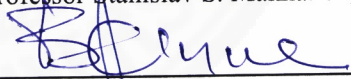
(Assistant Professor Pakinee Aimmaree, Ph.D.)

Co-Advisor



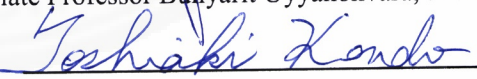
(Professor Stanislav S. Makhanov, Ph.D.)

Committee Member and Chairperson
of Examination Committee



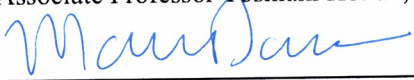
(Associate Professor Bunyarit Uyyanonvara, Ph.D.)

Committee Member



(Associate Professor Toshiaki Kondo, Ph.D.)

Committee Member



(Associate Professor Matthew N. Dailey, Ph.D.)

External Examiner: Professor Rangaraj M. Rangayyan, Ph.D.

DECEMBER 2016

Abstract

OPTIC DISK DETECTION AND SEGMENTATION APPROACHES BASED ON VESSEL NETWORK

by

NITTAYA MUANGNAK

B.S. (Computer Science), Mahasarakham University, 2001

M.S. (Computer Science), Chiang Mai University, 2004

Precise localization of the optic disk (OD) in retinal images is one of the challenges in ophthalmic image processing. Although many efforts have been made towards finding automated numerical solutions, they often fail on retinal images characterized by poor quality. Therefore, we introduce three novel methods namely, Vessel Transform (VT), Vessel Vector based Phase Portrait Analysis (VVPPA), and Hybrid Approach (HA) for automatic detection of the OD based primarily on retinal blood vessels. To localize OD, VT finds a set of solution in an image space that yields the smallest sum of distance from a solution point to clusters of vessels. VVPPA uses convergence points obtained from Phase Portrait Analysis (PPA) operated on vectors derived from vessels to get the location of OD. The HA uses a set of rules obtained from a decision tree to alternate using VT and VVPPA. These three methods are integrated with the scale space approach (SS) to obtain the OD boundary. The integration of VT, VVPPA, and HA with SS is defined by SSVT, SSVVPPA, and SSHA, respectively. The new algorithms have been tested against the existing methods: fuzzy convergence and circular transform. The numerical experiments demonstrate that our proposed algorithm outperforms the existing methods, especially on poor quality images. For localization of the OD, the HA gets the highest accuracy of 98% regardless of poor image quality and satisfactorily comparable with the existing method for the fair ones. For OD segmentation, all approaches are generally better than the existing methods.

Specifically, SSVT obtains the highest positive predictive value (PPV) of 79.22% while SSHA gets the highest sensitivity of 53.05%, respectively for poor quality images.

Keywords: Optic disk detection, optic disk localization, optic disk segmentation, vessel network, vessel transform, vessel vector based phase portrait analysis, hybrid approach



Acknowledgements

I kindly acknowledge to following supporters who have contributed to my work throughout my Ph.D. study.

Firstly, I would like to express my sincere gratitude to my advisor Asst. Prof. Dr. Pakinee Aimmanee for her kindly support during my research, for her determination, motivation, encouragement, and tremendous comprehension. Her supervision helped me in all the time throughout the research including writing of this dissertation. I could not have imagined having a superior advisor for my doctoral study.

Besides my advisor, I would like to express my great appreciation to my co-advisor Prof. Dr. Stanislav S. Makhanov for his constructive guidance, enthusiastic encouragement, and useful critiques during the planning and development of this research. Productive advices given by him have been a great help in the research progression. His willingness to give his time so generously has been very much appreciated.

I would like to thank the rest of my thesis committees: Assoc. Prof. Dr. Bunyarit Uyyanonvara, Assoc. Prof. Dr. Toshiaki Kondo, and Assoc Prof. Dr. Matthew N. Dailey, for their insightful comments and encouragement in keeping my progress on schedule. My appreciation is also extended for their interesting questions which incented me to broaden my research from varying perspectives. I would also like to express my appreciation to my external examiner, Prof. Dr. Rangaraj M. Rangayyan, for his useful and insightful suggestions including all editors and reviewers who have commented my research publication.

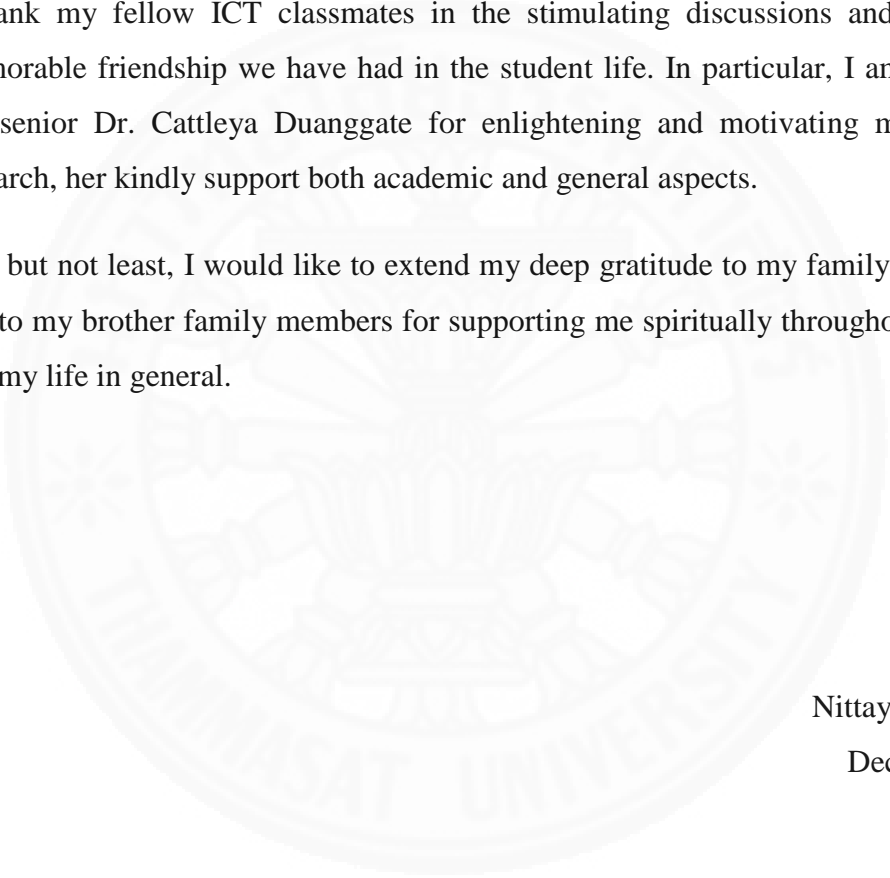
I also wish to thank the Thai Royal Government Scholarship, the Ministry of Science and Technology for fully providing financial support including Thailand Research Fund, and Center of Excellence in Biomedical Engineering of Thammasat University for the partially financial support.

My sincere thanks are extended to the SIIT staffs for offering me useful research facilities during working at the ICT graduate laboratory. Without their precious support it would not be possible to conduct this research.

I would like to acknowledge the help provided by Department of Ophthalmology, Faculty of Medicine of Thammasat University for the assistance with the data collection.

I thank my fellow ICT classmates in the stimulating discussions and for all the memorable friendship we have had in the student life. In particular, I am grateful to my senior Dr. Cattleya Duanggate for enlightening and motivating me on doing research, her kindly support both academic and general aspects.

Last but not least, I would like to extend my deep gratitude to my family: my parents and to my brother family members for supporting me spiritually throughout my study and my life in general.

The seal of Thammasat University is faintly visible in the background, centered on the page. It features a central emblem with a crown and two figures, surrounded by the text 'THAMMASAT UNIVERSITY' and Thai script.

Nittaya Muangnak
December 2016

Table of Contents

Chapter Title	Page
Signature Page	i
Abstract	ii
Acknowledgement	iv
Table of Contents	vi
List of Figures	ix
List of Tables	xii
List of Symbols and Acronyms	xiii
Chapter 1 Introduction	1
1.1 Importance	1
1.2 Retinal Images	2
1.3 Problem Statement	4
1.4 Purpose of Study	6
1.5 Thesis Arrangement	6
Chapter 2 Related Works	7
2.1 Literature Review of Optic Disk Detection	7
2.1.1 OD Feature-based Approach	7
2.1.2 Vessel-based Approach	12
2.2 Background	15
2.2.1 Phase Portrait Analysis (PPA)	15
2.2.2 Scale Space Approach (SS)	17
Chapter 3 Vessel Transform	19
3.1 Vessel Clustering	20
3.2 Vessel Transform	28

3.3	Scale Space Algorithm with VT for OD Segmentation	30
3.4	Advantages of the VT Approach	32
3.5	Disadvantages of the VT Approach	32
Chapter 4 Vessel Vector based Phase Portrait Analysis		33
4.1	Vectors involved in this Approach	34
4.1.1	Shifted Leading Vectors	34
4.1.2	Sole Vessel Vectors	34
4.1.3	Mahfouz Vectors	35
4.1.4	Bouncing Vectors	37
4.1.5	Interpolation Vectors	37
4.2	Vessel Vector based PPA Algorithm	39
4.3	Scale Space Algorithm with VVPPA for OD Segmentation	42
4.4	Advantages of the VVPPA Approach	44
4.5	Disadvantages of the VVPPA Approach	44
Chapter 5 Hybrid Approach for OD Detection		46
5.1	Hybrid Approach	46
5.2	Advantages of the Hybrid Approach	48
5.3	Disadvantages of the Hybrid Approach	48
Chapter 6 Experimental Setup and Evaluation Schemes		49
6.1	Retinal Fundus Image Collections	49
6.2	Retina Vessel Extraction Software	51
6.3	Ground Truth	52
6.4	Settings	53
6.4.1	For VT Approach	52
6.4.2	For VVPPA Approach	52
6.4.3	For SSVT Approach	53
6.4.4	For SSVVPPA Approach	54

6.4.5	For Hybrid Approach	55
6.5	Evaluation	56
6.6	Experiment	57
Chapter 7 Experimental Results and Discussion		59
7.1	Numerical Experiments of the Approaches in Locating the OD	59
7.2	Numerical Experiments of the Approaches in Detecting the OD Region	62
7.3	Discussions	66
Chapter 8 Conclusions and Recommendation for Future Work		69
8.1	Thesis Summary	69
8.2	Recommendation for Future work	71
8.3	Other perspectives	71
References		73
Appendix A		81

List of Figures

Figures	Page
1.1 The structure of an eye	3
1.2 A normal fundus image	3
1.3 An abnormal fundus image (OD swelling and hard exudates)	4
1.4 Example of poor quality images. Poor focus and clarity due to dimness (upper left). Poor optic disk visibility due to uneven illumination over it (upper right). Edge haze (lower left and right).	5
2.1 Phase portrait flow patterns [62], [63]	16
2.2 Scale-space OD detection. Left are original images after blurring with different scales and right are blobs obtained from that corresponding scales.	18
2.3 The combination of all significant blobs over multi scales	18
3.1 Vessel transform combined with the scale-space segmentation	19
3.2 The original image (top left), extracted vessels (top right), segmented vessels (middle left), removing short, thin or faint vessels (middle right), clustering (bottom left), removing small clusters (bottom right).	22
3.3 Convergence test	23
3.4 Quadratic regression for the threshold selection for the ROP data set	25
3.5 Quadratic regression for the threshold selection for the STARE data set	26
3.6 Illustration of Vessel Transform Calculation at two sample points P1 and P2 on the 5 isolated clusters. Clearly, $VT(P2) < VT(P1)$.	29
3.7 The original retinal images (left) and their corresponding VTs (right).	29
3.8 The conventional SS decision tree	31
3.9 The SSVT decision tree	31
4.1 VVPPA combined with the scale-space segmentation	33
4.2 An example of bifurcation vessels	34
4.3 An illustration of a leading vector (red) and a shifted leading vector (green)	35
4.4 Illustration of how to construct a sole vessel vector	36

4.5	Illustration of how vectors from the probabilistic OD approach of Mahfouz are obtained. (a) original image (b) the greatest difference of number of pixels in vertical edge and horizontal edge. (c) y-location vs the maximum number of bright pixels in a reference square at x-location. (d) the Mahfouz vectors.	37
4.6	A false XY-location obtained the Mahfouz's approach	38
4.7	Illustration of bouncing vectors of two original vectors	38
4.8	Illustration of steps in VVPPA algorithm	41
4.9	The SSVVPPA decision tree	42
4.10	Examples of OD rims obtained from SS (red solid) and SSVVPPA (blue solid) compared with ground truths (black solid) of six images	43
4.11	Examples of images that VVPPA fails due to insufficient information from the vessels. Green rectangle shows OD location obtained from VVPPA.	44
5.1	The OD localization and segmentation using HA	46
6.1	Examples of "fair" and "poor" images from ROP	50
6.2	Examples of "fair" and "poor" images from STARE	50
6.3	Extracted retinal vessels using ARIA	51
6.4	Illustration of finding the voting overlapping score from GT contours (blue, red, and green circles are given GT contours obtained by the first, second, and third experts, respectively)	52
6.5	Decision model of leading vector classification for ROP, red – data of the leading vectors and blue – data of the nonleading vectors	54
6.6	Decision model of leading vector classification for STARE, red – data of the leading vectors and blue – data of the nonleading vectors	54
6.7	SSVT decision trees for test collections: (left) ROP collection and (right) STARE collection	55
6.8	SSVVPPA decision trees for test collections: (left) ROP collection and (right) STARE collection	55
6.9	Decision system model of hybrid approach for OD localization	56
6.10	The four values demonstration as set	57
7.1	Examples of OD locations obtained from different approaches on eight images, Ground truth –black solid line, FC – green circle, CTM – blue square, VT – red triangle, VVPPA – pink diamond, and Hybrid Approach –white hexagon.	61

7.2	Examples of OD regions: 1-ground truth, 2-SSVT, 3-SS, 4-CTM, and 5-SSVVPPA, or 6-SSHA	63
7.3	Inconclusive cases by VT (red triangle) and SSVT (blue circle) approaches	66
7.4	Inconclusive cases by SSVVPPA approach	67
7.5	Inconclusive cases by HA (both VT and VVPPA): Green square - HA and black line - GT	68
8.1	Illustration of an alternative way to construct vectors	72



List of Tables

Tables	Page
2.1 Configuration types of 2-D critical points	16
3.1 Threshold values used in vessel clustering	27
6.1 Classification of the images into fair and poor	50
7.1 Accuracy of the OD location using FC, CTM, VT, VVPPA, and Hybrid Approach	62
7.2 Accuracy of the OD segmentation using CTM, SS, SSVT, SSVVPPA, and SSHA	62
7.3 The computational time CTM vs. our proposed approaches	66

List of Acronyms

ARIA	Automated Retinal Image Analyser
ASM	Active Shape Model
BV	Bouncing Vectors
BifV	Bifurcation Vectors
CTM	Lu's Circular Transform Method
DR	Diabetic Retinopathy
FC	Fuzzy Convergence
FN	False Negative
FP	False Positive
GT	Ground Truth
GVF	Gradient Vector Flow
HA	Hybrid Approach
IV	Interpolation Vectors
MOPH	the Ministry of Public Health
MV	Mahfouz Vectors
OD	Optic Disk
PCA	Principle Component Analysis
PPA	Phase Portrait Analysis
PPV	Positive Predictive Value
RBF	Radial Basis Function
ROP	Retinopathy of Prematurity
SLV	Shifted Leading Vector
SS	Scale Space Algorithm
SSHA	Scale Space Algorithm with HA
SSVT	Scale Space Algorithm with Vessel Transform
SSVPPA	Scale Space Algorithm with Vessel Vector based PPA
STARE	STructured Analysis of the REtina
SVM	Support Vector Machine
SVV	Sole Vessel Vectors
TN	True Negative

TP	True Positive
VT	Vessel Transform
VVPPA	Vessel Vector based Phase Portrait Analysis



Chapter 1

Introduction

1.1 Importance

The Thai Health Promotion Foundation revealed in 2014 that Thailand faces the problem of a severe lack of ophthalmologists. Nationwide, Thailand has only 1,080 registered ophthalmologists as of 2014 [1]. Seventy five percents of these ophthalmologists work at big hospitals in Bangkok and nearby provinces, or in the main cities of the larger provinces. In comparison, the eye patients within the age ranges of over 35 and under 70 years that are recorded by the Ministry of Public Health (MOPH) are 19% and 40%, respectively.

Unfortunately, 88% of these patients live in rural areas. Since the number of eye patients is currently increasing by around 7% per year [2], the lack of ophthalmologists, particularly in rural areas, is an ever increasing problem.

One instance of an eye disease that can be prevented by early diagnosis and treatment is diabetic retinopathy (DR). According to the statistics of the patients having diabetes aging between 15-34 years old across the country provided by the MOPH, the number of diabetics is as high as 49.73% and one tenth of this number is very likely to have DR [3]. Due to the small number of trained ophthalmologists and the poor provision of services and costly equipment in rural areas, the ability of doctors to diagnose and manage DR in the population is being severely impacted.

The OD is one of the crucial points in a retina. It is also important for establishing a frame of reference to detect regions of clinical importance inside a retinal image, such as the fovea or macula, and also to diagnose abnormalities of eye diseases. The OD usually appears in healthy retinal images as a bright, yellowish, circular, or oval object. The relative size of the OD in a fundus image depends on the field of view of the fundus camera or image, which the OD itself is partly entered by optic nerves. For example, the size of the OD in fundus images on a specific 35 degree field of view appears roughly one-sixth the width of the images in diameter [4] relative to the

images in healthy eyes. Any irregularity in the appearance of the OD is a sign of abnormalities or diseases such as glaucoma, DR or hypertensive retinopathy [5].

One in ten people are advised for annual retinal screening because of a variety of medical conditions [6]. However, annual retinal screening is nearly impossible in many developing countries due to the lack of trained specialists compared to the size of the diabetic population. This implies the necessity of automatic screening systems to assist ophthalmologists in diagnosing an early stage of diseases such as glaucoma and DR using computer-based identification. Since fundus imaging is a frequent clinical procedure, retinal fundus images are commonly used for a preliminary diagnosis and detecting suspicious cases.

The existing OD detection algorithms have typically been tested primarily on good quality retina images obtained from standard lab equipment that is achieving high accuracy. In this work, we develop three novel OD detection algorithms based on the information of vascular network rather than that of OD itself. These algorithms have been shown to detect OD with high accuracy in both fair and poor quality scenarios.

1.2 Retinal Images

The human visual system is mainly separated into three principal parts: the globe (see Figure 1.1), visual pathways (e.g. cornea, iris, lens, retina, optic nerve), and the visual cortex, which is the part of the brain dedicated to visual processing [7]. The outer part of the eye that provides protection for the globe and optical surface distortion is the eyelid. The refraction of the lens and the cornea act in unison to adjust the focal length to focus incoming light from objects clearly on the retina at any range.

The retina is the interior surface of the eye. The central field of vision, macula, is the focal point (see Figure 1.2) with regard to acuity of vision and its center is the fovea. The optic nerve transmits neuronal signals to the brain where the retinal ganglion cell axons are arisen. The axons stretch out through the convergence notch inside the OD alongside main retinal blood vessels found in the conjunctive vicinity of the OD [8].

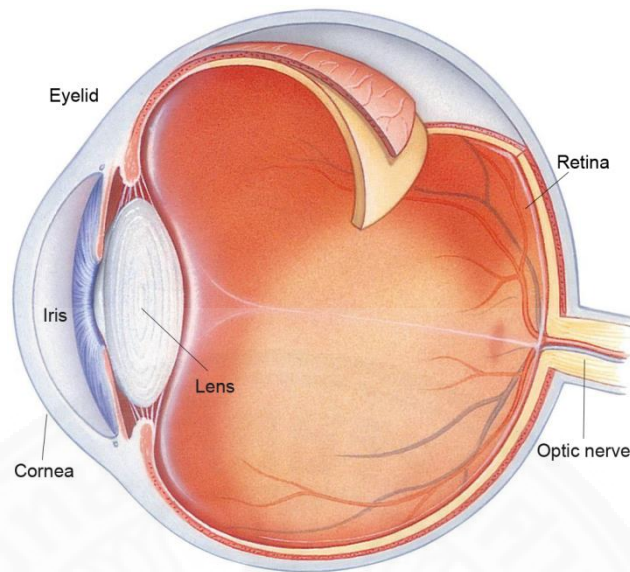


Figure 1.1: The structure of an eye
 (Image obtained from <http://www.human-anatomy99.info/internal-structure-of-the-eye/>. Accessed date: 7 December 2014.)

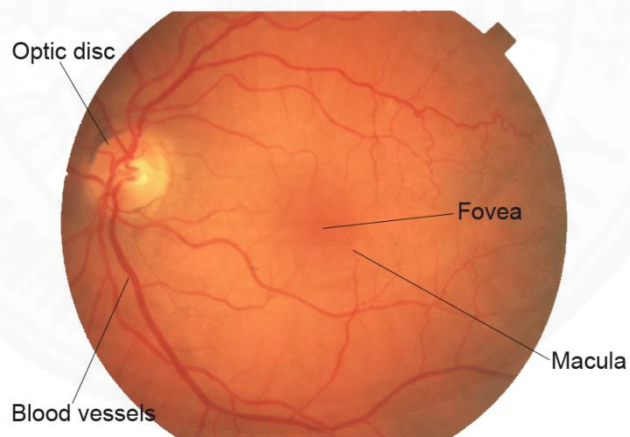


Figure 1.2: A normal fundus image

Early vision loss monitoring begins with an ocular fundus photograph taken by a fundus camera, documenting the appearance of the retina, retinal vessels, macula, fovea and OD. Ophthalmologists examine these digital fundus images for abnormalities, and assess their severity. Figure 1.2 and Figure 1.3 show the fundus images of normal and abnormal cases, respectively.

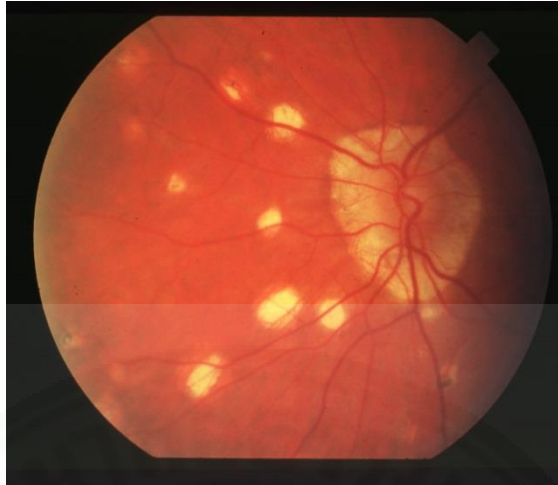


Figure 1.3: An abnormal fundus image (OD swelling and hard exudates)

The abnormal physical appearance of OD, fovea, macula, and blood vessels as well as the appearance of unusual components such as cotton wool, hemorrhages, exudates are often signs of abnormalities in the patients. They can be used to diagnose eye diseases, for instance, DR, hypertension (caused glaucoma), macular degeneration, and papilloedema [9].

1.3 Problem Statement

Many automatic optic disk detection techniques have been proposed [10][11][12][13][14][15]. Most of these techniques utilized features of OD such as size, shape, brightness, grey level, and contrast with background. The existing approaches can often do very well in detecting OD in good quality images of healthy patients, in some cases reporting accuracies of up to 100%. However, the major limitations of these approaches are that they typically only work well with good quality images, where the OD is clearly visible and contains the expected features. Poor quality images, or those taken from patients with retinal disease which causes abnormal changes to the appearance of the OD, often cause these methods to fail. Figure 1.4 shows examples of images in which the existing methods fail to find OD.

Two important facts about the vascular network that can be used to localize OD are firstly that OD is the convergence of the vascular network; the vascular networks are usually present and traceable even poor quality images, or images with abnormal ODs. Poor quality fundus images originates from various factors such as poor focus, small pupil size, and media opacity.

Some previously proposed OD detection techniques have used vascular structure analysis, but without considering the hierarchical structure of the vessels. Thus, there are still improvements needed in these approaches in order to precisely locate the OD in these difficult cases.

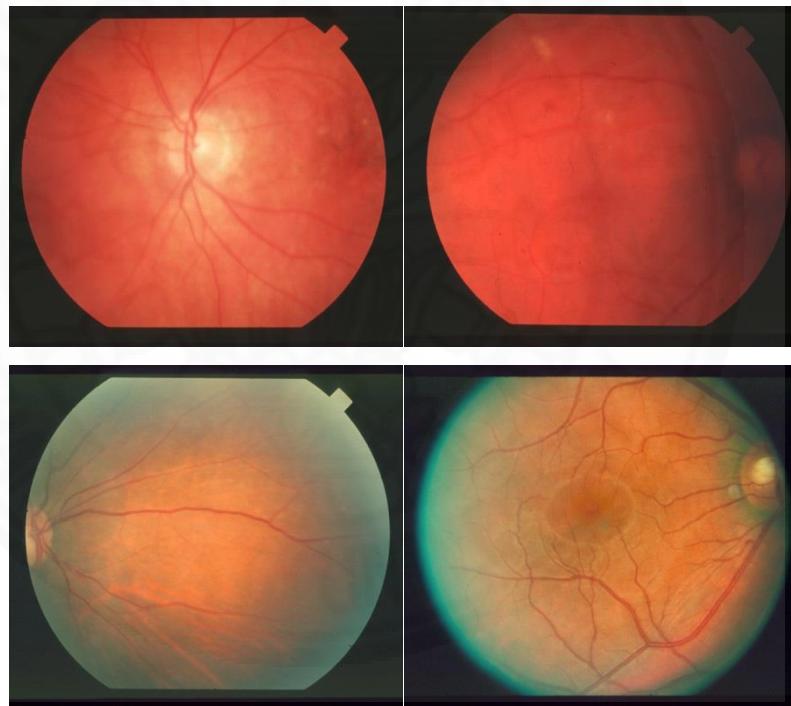


Figure 1.4: Example of poor quality images. Poor focus and clarity due to dimness (upper left). Poor optic disk visibility due to uneven illumination over it (upper right). Edge haze (lower left and right).

1.4 Purpose of Study

The purposes of this work can be summarized as follows. First is to present three novel approaches for automatically localizing the OD in fundus images, namely vessel transform (VT), vessel vector based phase portrait analysis (VVPPA), and the hybrid approach (HA). Second is to integrate the proposed OD localization methods with the scale space approach (SS) to segment the boundary of the OD. Last is to compare and discuss the results of the proposed methods with other existing methods for two different quality image collections: fair and poor.

1.5 Thesis Arrangement

This thesis is arranged into eight chapters as follows. This chapter provides background, retinal image characteristics in human eyes, problem statement, and purpose of the study. Chapter 2 provides literature reviews on automatic optic disk localization, segmentation approaches, and related background. Chapter 3 describes our first approach to localize optic disk using the vessel transform (VT) technique. Chapter 4 describes our second approach which detects optic disk based on vectors derived from vessels. The novel hybrid approach (HA) derived from these two techniques is discussed in Chapter 5. Chapter 6 describes the image collection as well as evaluation schemes used in our experiment. Corresponding experimental results including discussions of the study are stated in Chapter 7. Chapter 8 which is the last chapter summarizes the whole thesis work and provides plans of the future work including other perspectives.

Chapter 2

Related Works

In this chapter we review the current methods of OD detection in the literature. First we review the two main OD detection approaches in Section 2.1, which can be categorized into feature-based and vascular-based methods. Section 2.2 then reviews the theory behind the Phase Portrait Analysis and the Scale Space algorithm, which are employed in our proposed novel approaches.

2.1 Literature Review of Optic Disk Detection

2.1.1 OD Feature-based Approach

The main assumptions of conventional OD detection techniques are typically that it is roughly central in the image, appears as a bright circular region with high grey level variation (entropy), and whose size falls within a limited range. Typically the OD is defined in the literature as the largest bright pixel cluster present in retinal images, therefore the previously mentioned features are often used in conventional OD detection approaches.

Lalonde et al. [10] and Jelinek et al. [11] proposed template matching and Haar transform to localize the OD. Multi-resolution image decomposition [10] was investigated to provide aggregated pyramidal candidate regions. A circular-like object was determined using the Canny edge detection [11] and prior information was then defined as the OD tracking template. The candidate region possessing the optimum distance to the template was selected as the OD segmentation result. Niemeijer et al. [12] presented an automatic system to detect the location of the OD and fovea in color retinal images. To locate OD, a k-Nearest Neighbor regression and a circular template were applied to estimate the distance to the object of interest at any given location in the image based on a set of features measured at that location. Another robust method for localizing the OD center in presence of pathological regions was proposed by Deghani et al. [13]. Histograms of each color component were used as templates for OD localization. Histogram matching by correlation was used to obtain the binary

image containing the attracting force field of vessel density which converges as the OD.

Cox and Wood proposed an edge detection technique to obtain points on the OD boundary which were then automatically connected by a tracing procedure [14]. Morris et al. [15] presented a similar method which traces points characterized by large gradients.

A recent literature survey of Winder et al. [16] cited 38 papers on localization of the OD and identification of its boundary. The localization was most frequently achieved by PCA, active contour models (snakes) and watershed transforms. Several popular citations from the survey combined PCA and snakes. However, these segmentation techniques required well-validated algorithms to define the proposal component. This is why the conventional OD identification methods and an adaptive thresholding are still applicable.

Active contour models (snakes) were also applied to detect the OD in fundus images. The initial contour was initiated roughly to the optic nerve head location [17][18][19]. These models were reported to be successful in the images with high resolution and contrast. The main drawback of these algorithms was that it returns false boundary convergence caused by the noise and missing edges, most commonly seen in the infant images used for the detection of Retinopathy of Prematurity [20]. PCA and active contours were often combined to detect the OD center and to approximate the OD [21][22]. Lowell et al. [23] also simply performed a specialized correlated template matching by considering the reliable circular-bright object to localize the OD. The modified deformable models (active contour) were then applied to calculate the entire OD contour. The initial components of these active contour models were defined roughly by considering the object's brightest area, which was assumed to be the approximated OD center.

Akram and Kham [24] employed two basic features - intensity variation and grey level - to identify the OD and/or the presence of lesions. The OD rim was detected using the Hough transform, with a fuzzy hybrid neural network model proposed to

classify between the OD and lesions. Accuracies of up to 98 percent were demonstrated for various retinal image datasets. Despite the method being shown to be fast, simple and reasonably accurate, misidentified OD based on ideal features is still problematic when the OD rim is obscured due to high contrast retinal vessels, or image artefacts (blurring, shadows, noise, etc.). Besides, the precise OD identification based on the above-mentioned features could be highly delicate to pathological regions such as yellow/white lesions, exudates, or bright artifacts appearing on the retinal photographs [25][26]. Sinthanayothin et al. [27] used the specific intensity variation between the dark vessels and the bright nerve fibers to locate the OD. This procedure also located the fovea, and retinal blood vessels. However, the algorithm often failed to detect the OD in fundus images where a large number of white lesions were present.

Curvelet transforms have also been explored for solving the OD segmentation problem in [28][29]. The OD candidates were determined on bright circular objects that obtained large curvelet coefficients. Retinal vessel information was applied to validate the corresponding region with the strongest convergence as detected OD. A variational level set deformable model was then applied to segment the OD boundary. Shahbeig and Hossein [30] also combined the curvelet transform with the PCA and morphological operators based on geodesic conversions to obtain the OD region. Contrast enhancement of the image was performed using the adaptive curvelet coefficient to improve the algorithm's performance. The reconstructed image containing the OD region considered the maximum intensity of the circular regions obtained from adaptive correction function as the final OD. It was reported that these techniques failed in images where the OD appeared darker than the surrounding background.

Pereira et al. [31] analyzed the brightness of a series of images which were smoothed by an anisotropic diffusion filter, applying an "ant colony optimization" procedure to determine the OD contour from edge information. Local intensity variations were then used to initiate the iterative "ant pheromone" matrix, which is the same size as the retinal image, to search for feasible OD edges. This method was mostly concerned with finding the largest components revealed by the artificial ant colonies, without

considering morphological structure. This would cause unsuccessful reports in pathological images when the presence of large bright lesions, poor contrast, and other artifact is common. Morales et al. [32] also used PCA, stochastic watershed, and region discrimination. The preprocessed retinal image was manipulated by PCA to separate different object compositions. Blood vessels were suppressed by the inpainting technique and the desired OD edge was calculated by stochastic watershed transformation. It was found that the algorithm only performed well in cases where OD contrast was sufficiently high compared to the surrounding background, and also performed poorly in the images containing uneven shape and brightness in the OD.

Hsiao et al. [33] localized the OD by an illumination correction algorithm, with a supervised deformable model (GVF snake) and Circular Hough Transform being applied to segment OD boundary. Ramakanth and Babu [34] proposed OD localization based on an approximate nearest neighbor field. An initial single optic disk image was used as a reference dictionary to detect the OD. Feature Matching was then applied to find similarity of two patches: source and target. The location with the maximum likelihood was indicated to verify particular criteria and return OD center. This approach was parameter free and could handle any unseen database.

Giachetti et al. [35] proposed optic disk detection using the fast radial symmetry transform to determine circular bright objects with a particular radius. The bright symmetrical region corresponding to approximation correlations was taken as the candidate OD. The candidate with the highest vessel density feature had multiscale vessel inpainting applied, yielding the approximate OD location. Snake-based local refinement contour and ellipse contour refitting were integrated to obtain OD contour in this algorithm. The snake evolution was terminated when oscillations were detected. Nevertheless, the algorithm required a potential pre-processing step to provide well-defined and strong edge.

Kavitha et al. [36] used morphological operations and multilevel thresholding to extract the brighter regions that included the OD and exudates. Automatic detection of the optic nerve using digital red-free fundus photography was presented by Tobin et al. [37]. The location of the OD is depicted by a two-class Bayesian classifier.

Mathematical morphology techniques have been extensively applied for extracting feature components relevant to the OD thanks to their speed, as discussed in [38]. Li and Chutatape [5][21] used a combination of PCA and a point distribution model [39] tailored for active shape model (ASM) segmentation, with PCA being used to localize the OD and initialize the ASM. The OD boundary was detected using an iterative searching procedure called the modified ASM. We found that this algorithm was not applicable for the retinal images with either an absence of visible vessels in the OD or a faint, poor contrast OD boundary edge. A well-known method so-called the Circular Hough Transform was proposed in [40][41][42][43] to localize the OD. Sekhar et al. [40], Azuara-Blanco et al. [42], and Sagar et al. [43] detected the OD by finding the brightest region within the image. The size of the OD was calculated using morphological operations. The Circular Hough Transform was then applied to the gradient image to detect the contour and center of the OD. However, Zhu and Rangayyan [41] showed unacceptable performance of the Circular Hough Transform when the OD manifested slightly non-circular shape.

One of the most successful works tested against many existing algorithms is proposed by Lu [44]. Their modification of the circular transform combined with evaluation of the brightness was claimed to be more efficient, more accurate and faster than other state-of-the-art techniques such as the morphological approach proposed by Welfer et al. [45], a vessel's direction matched filter proposed by Youssif et al. [46], localization using dimensionality reduction of the search space proposed by Mahfouz and Fahmy [47], and genetic algorithms by Carmona et al. [48].

In general, the major drawback of the feature-based approaches is that they often incorrectly localize the OD when the OD's physical appearances such as shape, color, brightness or size become abnormal. The OD obscured by blood vessels or only partially visible (blur, shadows and noise) could be also misclassified. In addition, feature-based methods can be highly sensitive to other variable anatomical and pathological features often present in the retinal images [23].

2.1.2 Vessel-based Approach

Another well-explored subclass of OD detection algorithms are based on exploiting information from the vascular network directly. Many vessel-based OD localization techniques have quoted high accuracies in the literature [4][12][36][45][46][49][50][51][52][53][54][55][56][57][58][59]. Akita and Kuga [51] traced the parent-child relationship between blood vessels segments, tracking back to the center of the OD. In addition to brightness and shape features of the OD, Chaudhuri et al. [59] checked the area where vertically oriented vessels converged. To check the convergence, the vessels were treated as a single line of an infinite length. Consequently, the detection of the convergence area was reduced to a line intersection problem.

Automatic detection of OD and exudates in retinal images had been proposed by Kavitha and Devi [36] using a least square polynomial curve fitting algorithm to detect the OD through the convergence point of blood vessels. A multilevel thresholding technique was then applied to extract the bright regions. The point corresponding to the strongest vessel convergence region was examined as the OD center, otherwise exudates. As a matter of fact that retinal vascular network originates from the optic nerve head and their paths follow a parabolic shape. To describe the general direction of retinal vessels at any given position in the image, a geometrical parametric model was proposed by Foracchia et al. [49], where the directional vascular pattern in the retinal fundus images was unchanged and the model parameters was the OD coordinate center. Ravishankar et al. [50] also showed the approximate location of the OD where all major blood vessels intersect. The high intensity features of disk regions was combined to improve the robustness of the OD detection. The OD boundary was approximated as a circular mask, obtained using the Circular Hough Transform.

Chrastek et al. [52] determined the OD where the vertically oriented vessels converged together by the circular bright features. Dehghani et al. [53] identified the OD by finding the region containing the highest density of vessels, corners, and bifurcation points. This algorithm is rotationally invariant, but still required the presence of pathological regions to be distinguished, and needed sufficiently high

contrast between the OD and surrounding background to perform well. Youssif et al. [46] and Zhang and Zhao [54] introduced the directional vasculature based method to obtain the approximate OD location. Both works used the assumption about the horizontal alignment of the vascular network in the retinal images to extract high-priority identifying OD features. The vascular network was checked for the interception point between its centroid and the main vessels arcade fragments using sliding horizontal line [46]. The vessel distribution and global direction characteristics were combined to find the horizontal and vertical position of the OD. The general Hough Transform was then applied to obtain alternative parabolas and one fitting most of vessel pixels was identified as the OD center [54]. However, the limitations of these approaches are that they require complete vessel structures and/or they are not rotational invariant on retinal images. The entropy of the vascular directions was introduced in Mendonca et al. [55] approach to examine the incidents and the diversity of gradient orientations of vessel pixels. The idea of a multi-resolution sliding band filter was also extended in Dashtbozorg et al. work [56].

A number of effective tracing contour algorithms have been developed. Semashko et al. [58] employed the positions of the vessels to correct the pressure force of the active contour (snake) to improve the convergence to the OD. The Circular Hough Transform was used to initialize the circular contour approximation of the OD inside the edge map. The OD boundary was then utilized by the gradient vector flow (GVF) snake to generate the final OD edge map.

Although the vessel-based methods require a robust and accurate segmentation of the vascular tree, they perform well in the presence of poorly defined OD features (such as poor contrast boundaries, and pathological regions in or around the OD). The motivation of finding the vessel convergence area presents a considerable challenge. Consider the simplest case when the blood vessel segments are represented by line segments and the adjacency of those lines have been clustered. The focal point of the major clusters could point to the OD. However, in some cases, this assumption can lead to extremely inaccurate results. Many adjacent groups could be located far from the OD. Therefore, these vessel-based methods work out by partitioning the data set

into decisive (inliers) and indecisive (outliers) classes and require at least 50% of inliers [4][46].

The best performing vessel convergence technique was introduced by Hoover and Goldbaum [4]. The so-called “fuzzy convergence” (FC) method [60] created a fuzzy segment of which an area provided voting scores to corresponding pixels indicated the fuzzy score of each vessel. The voting score took place on the integer grid of the original image. An image map representing the strong point of the convergence of each pixel was calculated through the summation of votes at each corresponding pixel. The image map was then smoothed and the strongest convergence points obtained by thresholding. The FC technique was combined with a feature-based approach which employs illumination equalization to minimize the large intensity variation at different scales. The method verification on STructured Analysis of the REtina (STARE) database showed acceptable performance overall (89%), and 100 % success on the healthy images.

Phase portrait analysis (PPA) was modified to detect the OD in the retinal fundus images proposed by Rangayyan et al. [61]. This method decomposed trajectory patterns in term of parametric representation to classify the convergence configuration. The phase portrait modeled the oriented texture by means of eigenvalues into node and saddle maps along texture produced by Gabor filters. The condition on corresponding analysis windows was configured such as to characterize the node map, and label all possible peaks (ordered by magnitude) that could indicate a convergence of the blood vessels. The center of OD was then selected from the possible ranked peaks based on circular shape and corresponding intensity selection obtained from pre-processing of images. The OD detection using Gabor filters and PPA methods has been successfully applied to poor quality images. It was observed that the impact of blood vessel bifurcations leads to high responses in the node phase portrait map. However, this is not applicable for all cases because the structural blood vessels in pathological images converge at non-OD positions. The method is also computationally intensive, with computation times highly sensitive to the size of the convolution window. Despite the above methods reporting high success rates, there is still room for improvement in term of insufficient vessel information or asymmetrical

orientation. Nevertheless, the hierarchical structure of the retinal vessels and their importance were not considered whereas the vessel network consists of both primary and secondary structure of retinal blood vessels. Consequently, we improve this by providing the novel numerical models by means of the characteristics of hierarchical vascular structure.

2.2 Background

In this section we provide background of two methods that play important roles to our proposed method. The first is the Phase Portrait Analysis (PPA). It is the method that we employ to find the convergence of the vectors obtained from the vessel. The second is the base method for finding the region of the OD.

2.2.1 Phase Portrait Analysis (PPA)

The Phase Portrait Analysis (PPA) concept is commonly applied to model natural and physical phenomena by means of a vector field, or so-called “*gradient vector field*”. Its representative set of trajectories is a phase portrait. The use of this method is for characterizing eigenvalues of the corresponding linear flow matrix obtained from the first-derivative of specific function (the least square method). The PPA contributes the analysis of the possible trajectories or the phase portrait orientation force field by measuring parametric representation of strong flow patterns [62][63]. The flow patterns represent the series of oriented vector field. The following formula (2.1) is defined a phase plane of the oriented vector field in linear flow system by

$$\begin{aligned} x' &= ax + by \\ y' &= cx + dy \end{aligned} \quad \rightarrow \quad \frac{dv}{dt} = Av \quad (2.1)$$

where x' and y' indicates phase plane of vector field v , velocity $\frac{dv}{dt}$ is specified by the differential equation, and $A = \begin{pmatrix} a & b \\ c & d \end{pmatrix}$ obtained from a linear least square method. The linear flow matrix A is applied in the sampling window to convolve the entire phase plane and return two characterized eigenvalues: λ_1, λ_2 .

The flow pattern is characterized by the real and imaginary parts of the eigenvalues defined by $R_i = \text{Re}\lambda_i$, $I_i = \text{Im}\lambda_i$, respectively.

The measurement of the parametric representation determined by PPA defines the similarity of the vector field to match the particular pattern to the entire trajectory patterns [62][63]. The corresponding phase portrait linear flow patterns are demonstrated in Figure 2.1 and the basic linear trajectory patterns characterized by the flow matrix eigenvalues [64] is provided in Table 2.1.

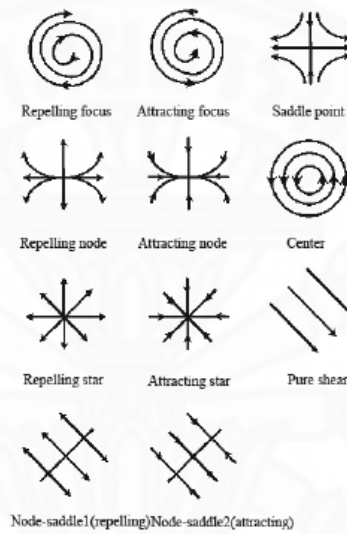


Figure 2.1: Phase portrait flow patterns [62], [63]

Table 2.1: Configuration types of 2-D critical points

Pattern	Eigenvalues after convoluting matrix A	
Center	$R_1 = R_2 = 0$	$I_1 = -I_2 \neq 0$
Attracting Focus	$R_1 = R_2 < 0$	$I_1 = -I_2 \neq 0$
Repelling Focus	$R_1 = R_2 > 0$	$I_1 = -I_2 \neq 0$
Attracting Node	$R_1 \neq R_2 < 0$	$I_1 = I_2 = 0$
Attracting Star	$R_1 = R_2 < 0$	$I_1 = I_2 = 0$
Repelling Node	$R_1 \neq R_2 > 0$	$I_1 = I_2 = 0$
Repelling Star	$R_1 = R_2 > 0$	$I_1 = I_2 = 0$
Saddle Point	$R_1 > 0, R_2 < 0$	$I_1 = I_2 = 0$
Node-Saddle 1	$R_1 > 0, R_2 = 0$	$I_1 = I_2 = 0$
Node-Saddle 2	$R_1 < 0, R_2 = 0$	$I_1 = I_2 = 0$
Pure Shear	$R_1 = R_2 = 0$	$I_1 = I_2 = 0$

Chucherd and Makhanov [65] proposed the trajectory pattern classifier to classify the sampling window into three areas of interest: noise, boundary, and regular points, given by,

$$C(W) = \begin{cases} \textit{noise}, & \frac{\min(|\lambda_1|, |\lambda_2|)}{\max(|\lambda_1|, |\lambda_2|)} > \Delta_1, & |\lambda_1| > \Delta_2 \textit{ or } |\lambda_2| > \Delta_2 \\ \textit{boundary}, & \frac{\min(|\lambda_1|, |\lambda_2|)}{\max(|\lambda_1|, |\lambda_2|)} < \Delta_1, & |\lambda_1| > \Delta_2 \textit{ or } |\lambda_2| > \Delta_2 \\ \textit{regular point}, & & |\lambda_1| \leq \Delta_2 \textit{ or } |\lambda_2| \leq \Delta_2 \end{cases} \quad (2.2)$$

where W is the sampling window around considered pixels and Δ_1, Δ_2 are the thresholds evaluated by feature selection method.

2.2.2 Scale Space Approach (SS)

The scale space theory was originally proposed by Witkin [66] to create a multiscale representation of signals in 1-D. Lindeberg [67] developed the SS to detect local maxima in 2-D intensity images at multiple scales into grey-level blobs. Identical blobs over all scales can be linked and represented into a scale-space blob tree. Relevant attributes such as lifetime, grey-level intensity, color, or contrast can be considered to obtain selected blobs by means of significant blob structure. The method is able to detect real-world objects at different observation scales.

A multi-scale representation of a two-dimensional images is defined by the scale-space method using the Gaussian smoothing kernel characterized by different variance (σ) value. Duangate et al. proposed an OD segmentation approach using Scale Space (SS) [68]. In their work, the blobs that exist over scales were linked and represented as a scale-space blob tree. The merging processes are applied to merge together the blobs that meet criteria of blob adjacency and also stability measured by relevant attributes. The merging process is repeated until the entire image contained stable number of significant blobs. Four attributes: size, brightness, intensity, and grey scale value were used as the relevant attributes in their work.

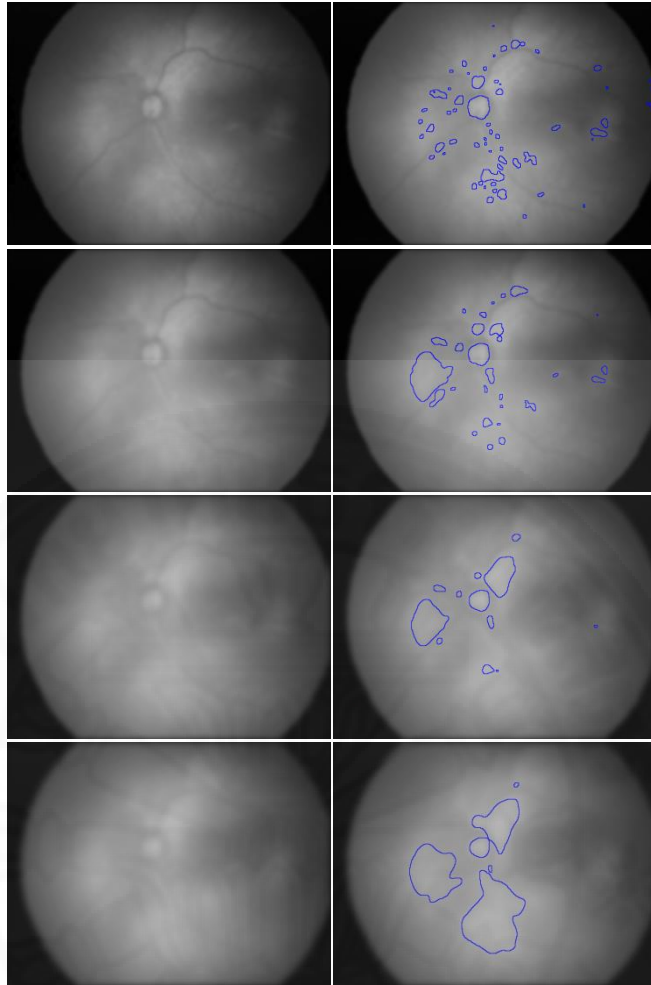


Figure 2.2: Scale-space OD detection. Left are original images after blurring with different scales and right are blobs obtained from that corresponding scales.

Figure 2.2 shows blobs that survive after the image was repeatedly scaled and the corresponding significant blobs over multiple scales in one plane are displayed in Figure 2.3. At a coarse level, all significant blobs which include an object of interest are kept. A subsequent classification method can be applied to all candidate blobs, giving the final desired blob.

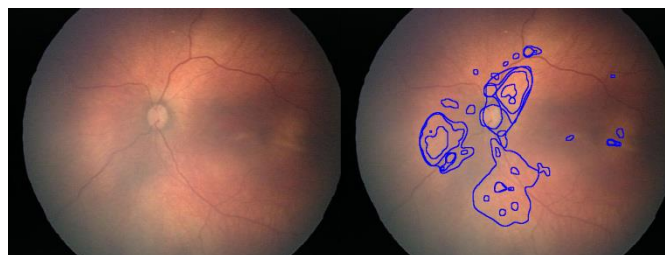


Figure 2.3: The combination of all significant blobs over multi scales

Chapter 3

Vessel Transform

This chapter introduces our first proposed approach, *vessel transform* (VT). We employed VT to localize the OD and used it as one of the features in the SS to obtain the rim of the OD. Figure 3.1 shows the overall process of the OD localization and segmentation using VT.

In this chapter, we define the vessel clustering algorithm to cluster vessels in section 3.1. The transformation of the vessel clusters to the distance space is defined in section 3.2. How VT is used in the SS algorithm for the OD segmentation is described in section 3.3. Section 3.4 and 3.5 provide advantages and disadvantages of the VT approach.

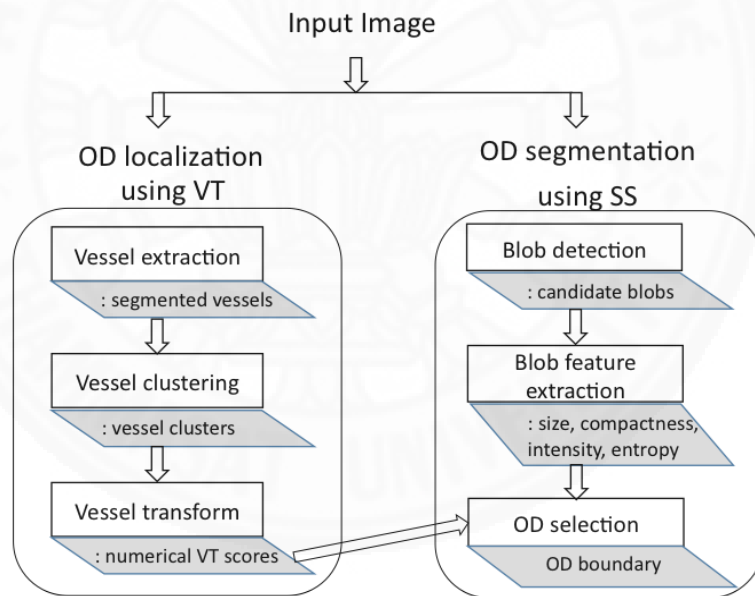


Figure 3.1: Vessel transform combined with the scale-space segmentation

3.1 Vessel Clustering

The vessels in the original images are first detected and extracted. The input of the clustering algorithm is a collection of vessels of size m (v_1, v_2, \dots, v_m), where m is an arbitrary integer. Each vessel, v_i , is represented by Cartesian coordinates of size N_i : $v_i = ((x, y)_{i,1}, (x, y)_{i,2}, \dots, (x, y)_{i,N_i})$. The collection of vessels can be obtained by a vessel segmentation algorithms, such as those defined by [69], [70], and [71]. To obtain the clusters, we applied the following algorithm.

The first three steps of our algorithm `Remove_Thin_Vessels(T_t)`, `Remove_Short_Vessels(T_l)`, and `Remove_Faint_Vessels(T_f)` are pre-processing designed to remove the outliers or unwanted vessels: thin, short, and faint vessels. It requires the following thresholds: T_t - the thickness threshold, T_l - the length threshold, T_f - the threshold on the gray level intensity of the vessel relative to the background. The fourth step merges the vessels into clusters and removes the isolated vessels. The merging step employs a threshold T_d on the maximum distance between clusters which can be merged into a new cluster. We apply a classical hierarchical bottom-up clustering. Initially the algorithm treats each vessel as a singleton $c_i = v_i$. Next, it successively merges clusters c_i and c_j if $dist(c_i, c_j) < T_d$ until they have been merged into several well separated sets. The final step, the post processing procedure detects and removes the outliers (small clusters) by checking the total thickness relied on vessel length as the cluster size. The condition $N_{c_i} < T_L$, where N_{c_i} denotes the size of the cluster c_i and T_L the corresponding threshold is exerted in this step.

The clustering step is based on the bottom up hierarchical approach. Initially the algorithm treats each vessel as a singleton cluster and then successively merges vessels until they have been merged into several well separated sets. Note that this type of clustering does not include time consuming of tracing procedures designed to detect the tree-like structure of the vessels. However, if trained, the algorithm returns

well separated clusters sufficient to generate a VT which localizes the convergence region and consequently the OD. Figure 3.2 illustrates the proposed clustering method.

Input:

Vessel network:

$V = \{v_1, v_2, \dots, v_m\}$ a collection of vessels

$v_i = \{(x, y)_{i,1}, (x, y)_{i,2}, \dots, (x, y)_{i,N_i}\}$ points belonging to vessel v_i

Thresholds:

T_t - the minimal thickness,

T_l - the minimal length,

T_f - the maximum intensity of the vessel relative to the background,

T_d - the maximum distance threshold used to join the vessels into clusters

N_{c_i} - the size of the cluster (the total thickness relied on length of the vessels)

T_L - the minimum size of the cluster based on summation of thickness.

Output:

$C = \{c_1, c_2, \dots, c_N\}$ the collection of clusters

Algorithm:

Remove_Thin_Vessels(T_t)

Remove_Short_Vessels(T_l)

Remove_Faint_Vessels(T_f)

#Initialize_Clusters

$C_i = \{V_i\}$

#Cluster the vessels

for $i = 1:|C|$

 for $j = i+1:|C|$

 if c_i or c_j is not empty and $dist(c_i, c_j) < T_d$

$c_i = c_i \cup c_j$

$c_j = \emptyset$

 endif

 endfor

endfor

#Compute_Cluster_Size

for $i = 1:|C|$

$N_{c_i} = 0$

 for $j=1:|V_{c_i}|$

$N_{c_i} = N_{c_i} + thickness(V_{c_i}[j]);$

 endfor

endfor

Remove_Small_Clusters(T_L)

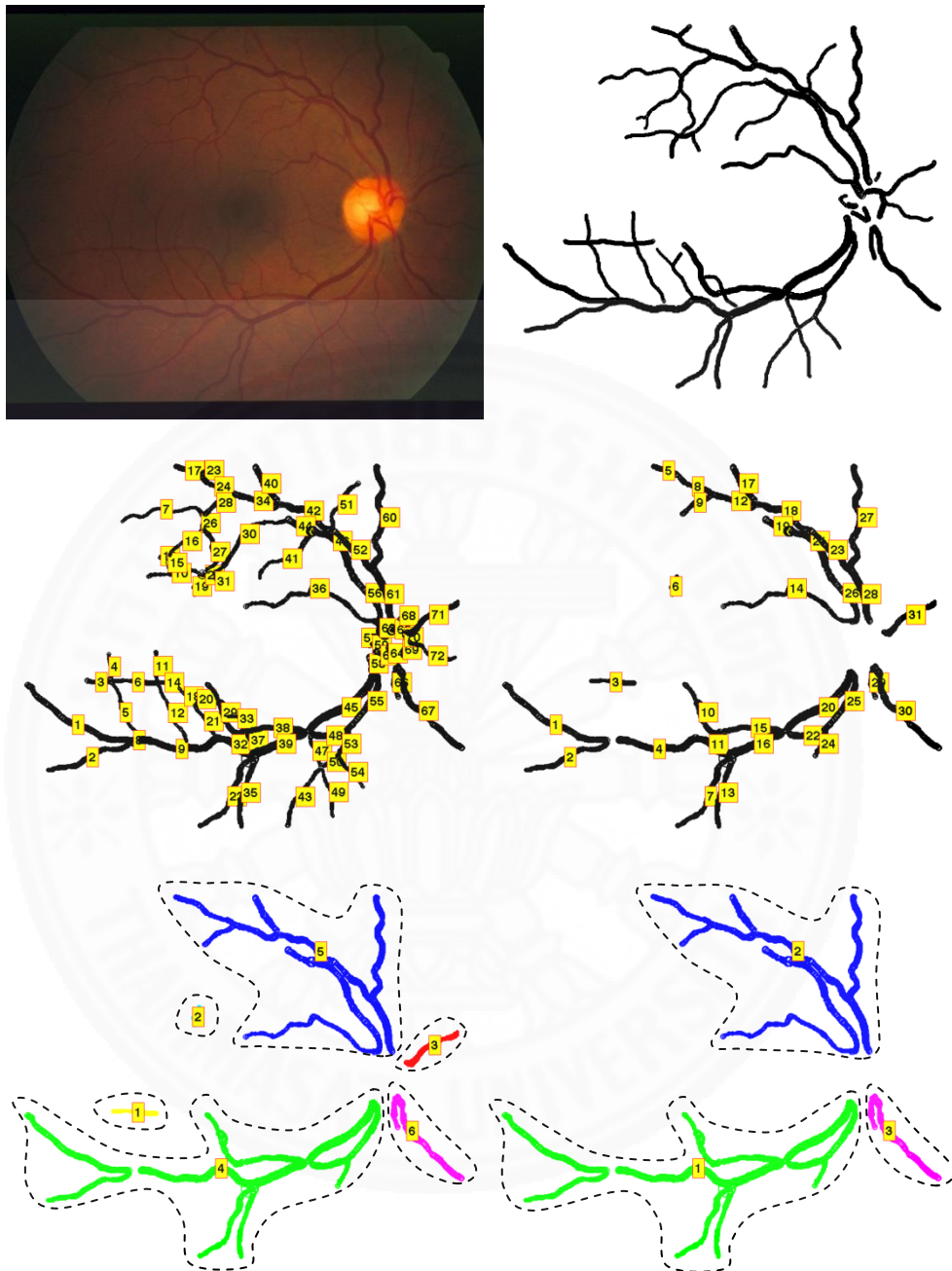


Figure 3.2: The original image (top left), extracted vessels (top right), segmented vessels (middle left), removing short, thin or faint vessels (middle right), clustering (bottom left), removing small clusters (bottom right).

The VT based OD localization requires that the resulting clusters converge to the OD. Therefore, for the images merged into three or more clusters, we verify the quality of convergence as follows. First, we evaluate the convergence region $\Omega = \operatorname{argmin}_p V(P)$ and its centroid. Next, the clusters are withdrawn one by one from the collection of clusters and re-evaluated the convergence regions Ω' corresponding to these new collections. If the minimum distance between the centroid of Ω and the new convergence regions Ω' is greater than the corresponding threshold T_Ω , the clustering is discarded.

The annotation of this condition is defined as following: $\operatorname{dist}(O_\Omega, O_{\Omega'}) > T_\Omega$, where O_Ω is the centroid of Ω , $O_{\Omega'}$ the centroid of Ω' and T_Ω the corresponding threshold. Our assumption is that if the vessels strongly converge to Ω , the system without one cluster converges approximately to the same region (see Figure 3.3). The second step is the evaluation of the convergence by $\min_{c_i} (\operatorname{dist}(c_i, \Omega))$, where c_i is the i^{th} cluster.

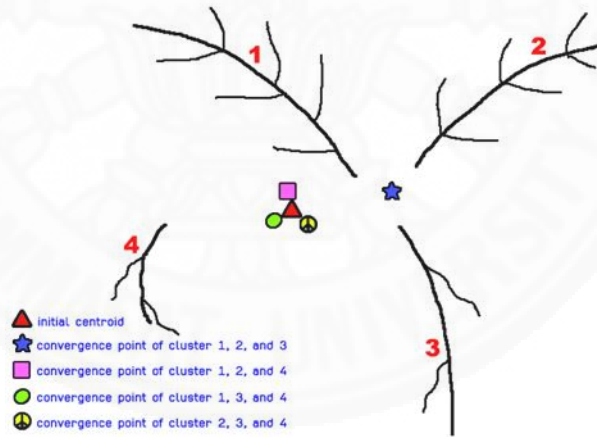
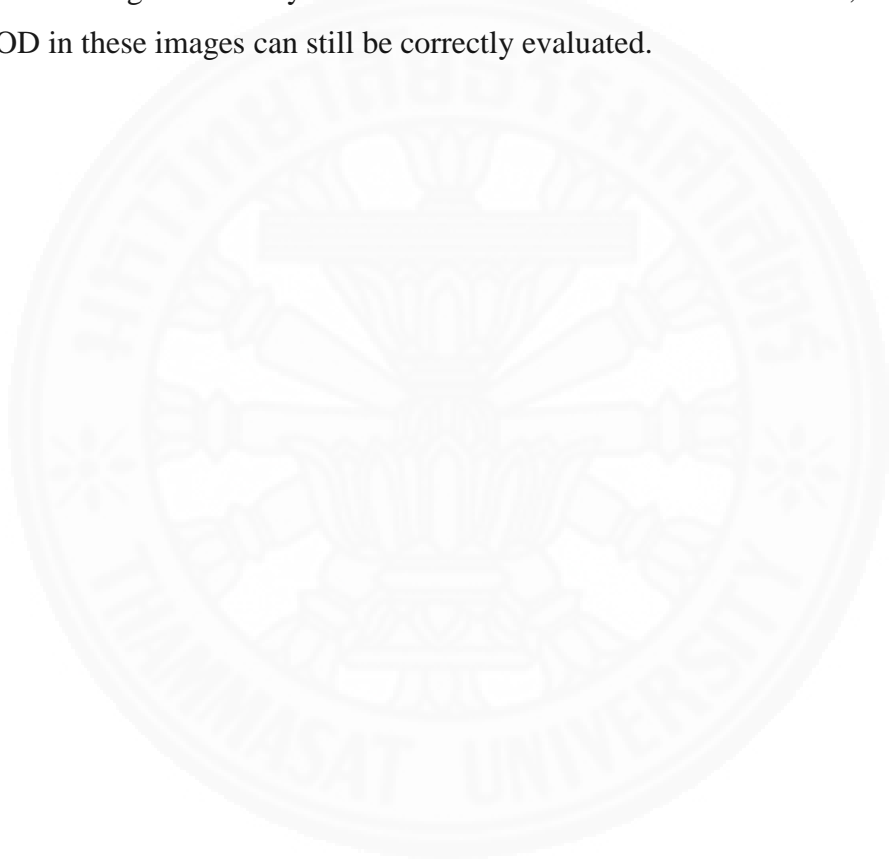


Figure 3.3: Convergence test

If $\min_{c_i} (\operatorname{dist}(c_i, \Omega)) < T_{VT}$, where T_{VT} is the corresponding threshold, the clusters are close enough to the convergence region Ω and the clustering is considered successful. In this case, the VT is included in the prescribed set of features for a further evaluation.

In a few cases the clustering algorithm returns an unacceptable result which consists of only one or two clusters. For such cases, we could not reliably test the convergence by excluding clusters (the first step). Technically, one can modify the thresholds and merge the vessels into a new set of clusters. However, testing an algorithm based on this idea is still an open problem. Therefore, following [68] we discard the VT feature and apply the scale space algorithm in its original version [66] (see also our forthcoming section 3.3). The numerical experiments show that the number of the discarded images is usually small and does not exceed 10%. Besides, the location of the OD in these images can still be correctly evaluated.



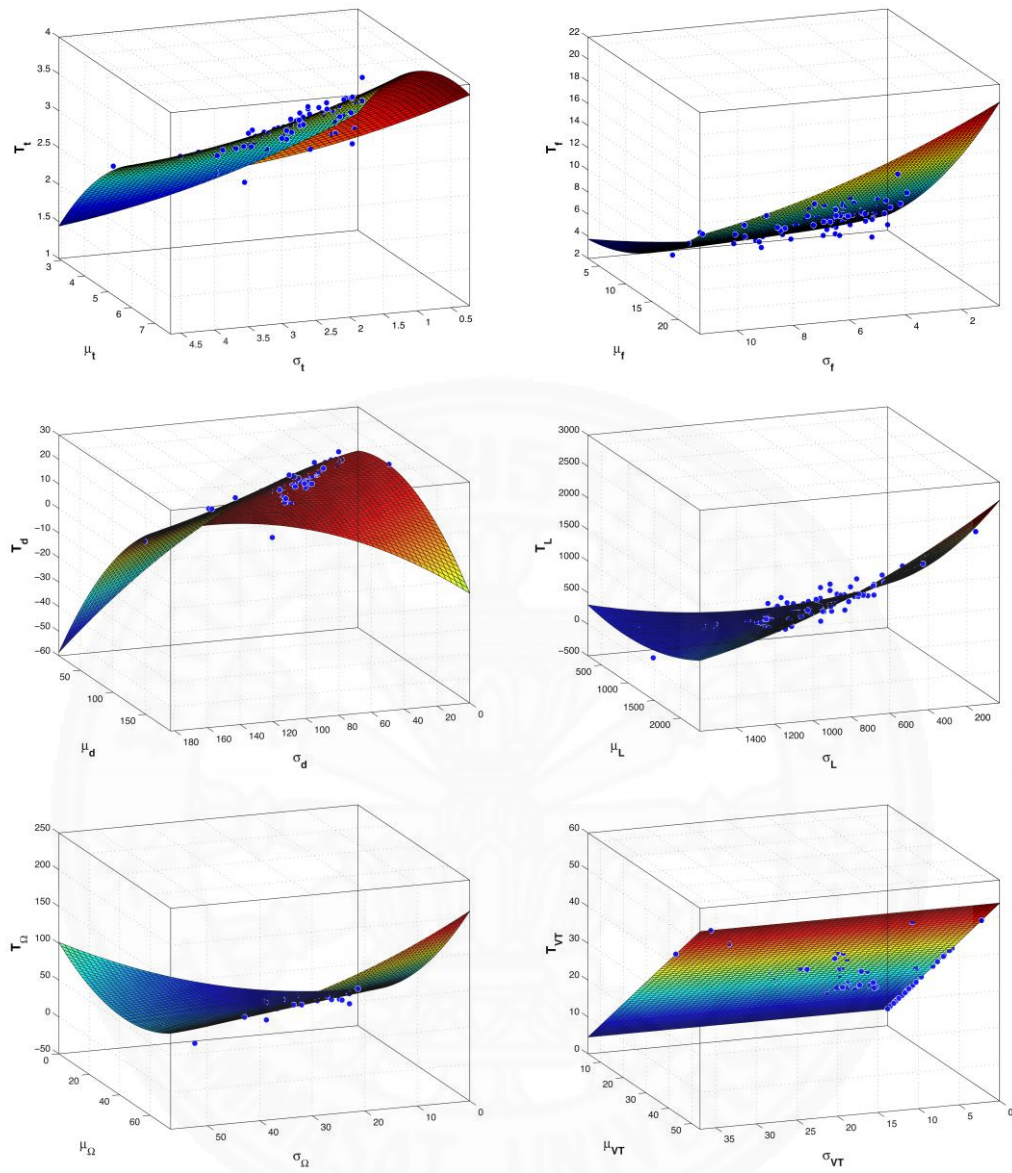


Figure 3.4: Quadratic regression for the threshold selection for the ROP data set

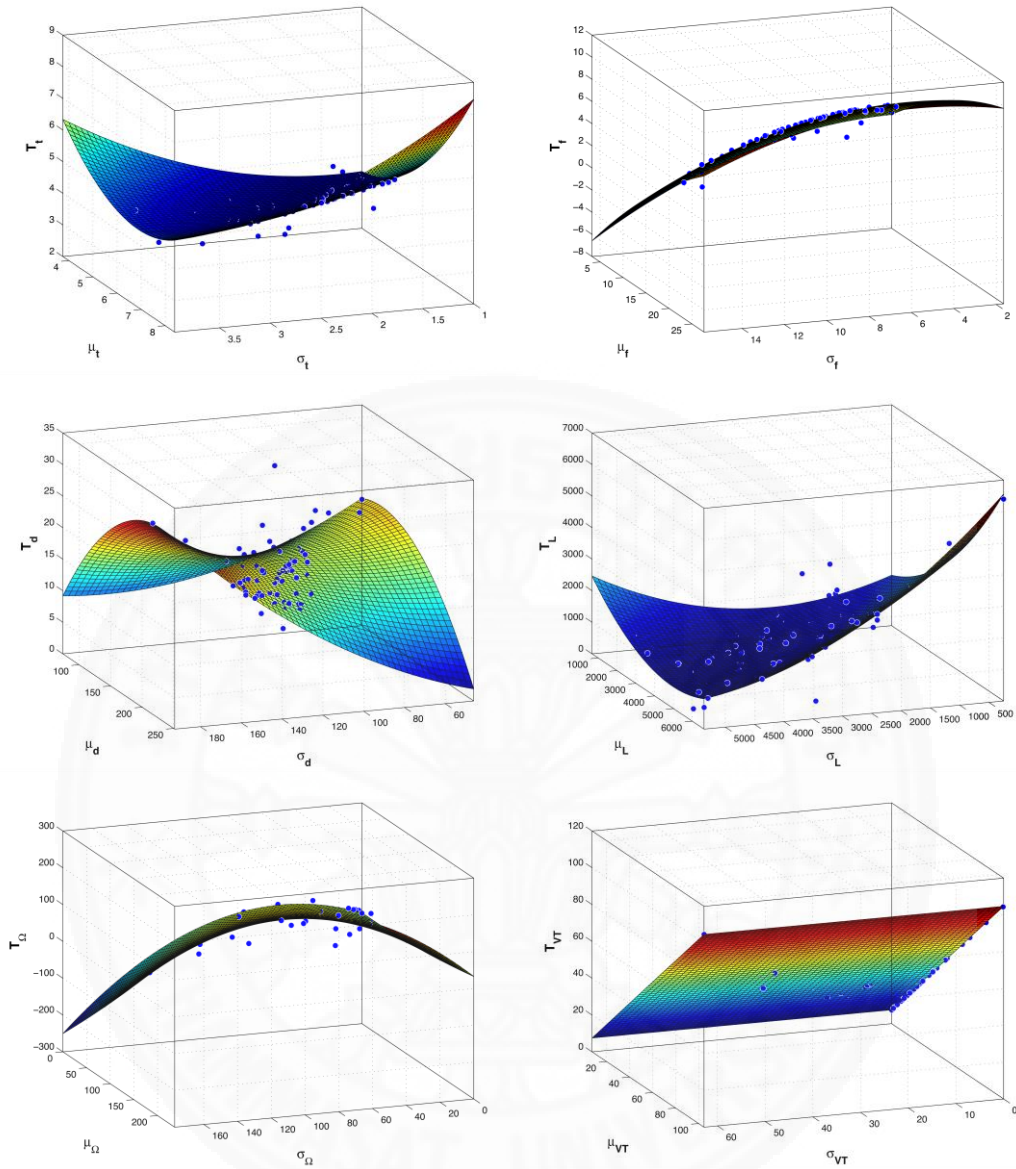


Figure 3.5: Quadratic regression for the threshold selection for the STARE data set

As mentioned above, the following thresholds: T_l - the minimal acceptable length of the vessel for a particular image (shorter vessels will be eliminated), T_t - the minimal acceptable thickness, T_f - the maximum acceptable intensity of the vessel relative to the background, T_d - the maximum distance between the clusters which can be merged

into a new cluster, T_L - the minimum acceptable size of the cluster, T_Ω and T_{VT} the thresholds used in the convergence test are required. The algorithm is trained using the bivariate quadratic approximation given by

$$T(\mu, \sigma) = a_1\mu^2 + a_2\sigma^2 + a_3\mu + a_4\sigma + a_5\mu\sigma + a_6 \quad (3.1)$$

where μ and σ are mean value and standard deviation of the corresponding parameter evaluated for a particular image. For instance, $T_l \equiv T_l(\mu_l, \sigma_l)$ is the threshold on the minimal acceptable length of the vessel, whereas μ_l is the mean length of a vessel in a particular image and σ_l is the standard deviation.

Our two collections of test images have been obtained by different devices with different lighting conditions. Therefore, they require different sets of thresholds which are obtained by the quadratic regression function (3.1). Figure 3.4 and Figure 3.5 illustrate the threshold selection applied to the ROP and the STARE set, respectively. We train the method using the classic 70-30% ratio between the training and the testing data. The resulting thresholds are given in Table 3.1.

Table 3.1: Threshold values used in vessel clustering

Data	Coef.	T_l	T_t	T_f	T_d	T_L	T_Ω	T_{VT}
ROP	a₁	0.13e-02	-0.76e-01	1.29e-02	-0.18e-02	0.18e-03	0.24e-01	3.92e-05
	a₂	0.88e-02	0.31e-01	0.38e-01	-0.15e-02	0.43e-03	0.31e-01	1.93e-06
	a₃	0.81e+00	1.07e+00	0.48e+00	2.04e-01	0.73e+00	1.11e+00	1.00e+00
	a₄	-0.13e+00	-0.47e+00	-0.30e+00	-0.18e+00	-0.46e+00	0.25e-01	-1.06e-04
	a₅	-0.13e-01	0.19e-01	-0.44e-01	0.35e-02	-0.66e-03	-0.55e-01	-3.66e-05
	a₆	2.09e+00	0.22e+00	2.14e+00	9.08e+00	2.85e+01	-0.71e-01	0.55e-01
STARE	a₁	-0.19e-02	0.19e+00	-0.66e-02	-0.88e-03	9.72e-05	0.65e-03	-2.17e-18
	a₂	-0.86e-02	0.35e+00	-0.43e-01	0.73e-03	0.16e-03	-0.18e-01	2.80e-17
	a₃	-0.41e+00	-0.86e+00	0.48e+00	1.15e-01	0.18e+00	-0.21e-01	1.00e+00
	a₄	0.99e+00	0.82e+00	0.81e-01	-0.36e+00	-0.59e+00	1.73e+00	4.40e-15
	a₅	0.84e-02	-0.45e+00	0.15e-01	0.15e-02	-0.21e-03	0.93e-02	-1.03e-16
	a₆	1.01e+01	4.85e+00	0.70e+00	2.64e+01	1.61e+03	1.32e+00	-6.99e-16

3.2 Vessel Transform

Given a collection of the vessel clusters using an algorithm defined in the earlier section, we apply VT to find the approximate location of OD.

The VT is given by

$$V(p) = \frac{1}{N} \sum_{i=1}^N \text{dist}(p, c_i), \quad (3.2)$$

where c_i is the i^{th} cluster of vessels, N is the number of clusters, $p = (x, y)$ is an arbitrary point in the image and $\text{dist}(p, c) = \min_{p' \in c} \|p - p'\|$.

Figure 3.6 illustrates how VT is calculated at a point. The shortest distances from P_1 to each cluster are shown in red whereas the shortest distances from P_2 to each cluster are shown in green. $V(P_1)$ is the average of the red distances and $V(P_2)$ is the average of the green distances. Ideally, the points in the neighborhood of OD obtains low values of V . To display this function within the range between 0 and 255 to better illustrate the distance in a grayscale, we normalized the $V(p)$ as follow.

$$V^*(p) = 255 - \frac{255}{V_{max}} V(p), \quad (3.3)$$

where p is a point in the image, V_{max} is the maximum value of $V(p)$ for all points in the image. In the vessel transformed space, the darkest area shows the location of the image that obtains the minimum value of VT. An introductory example in Figure 3.7 displays the sample retinal images and their corresponding VTs. Figure 3.7 illustrates how the minimum values are given by vessel transform.

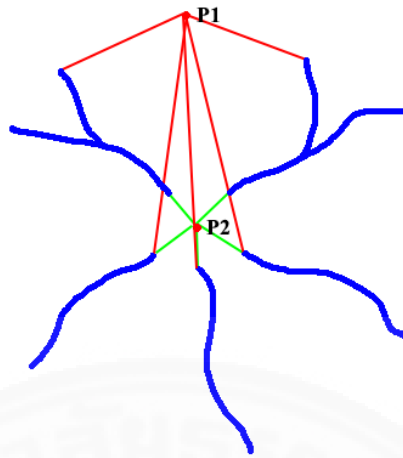


Figure 3.6: Illustration of Vessel Transform Calculation at two sample points P_1 and P_2 on the 5 isolated clusters. Clearly, $VT(P_2) < VT(P_1)$.

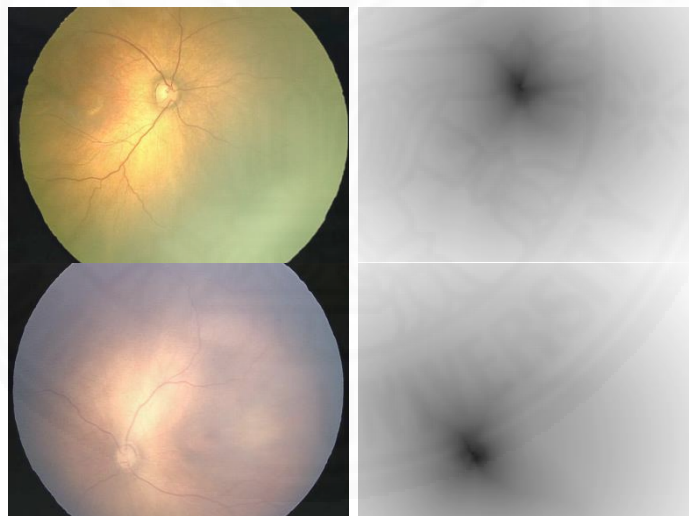


Figure 3.7: The original retinal images (left) and their corresponding VTs (right).

3.3 Scale Space Algorithm with VT for OD Segmentation

The VT alone generates only an approximated location of the OD. To obtain an exact boundary of the OD, we employ the OD segmentation method so-called SS [68] by integrating with the VT.

Duanggate et al. [68] used a scale space method to obtain and detect the OD in the retinal images. The method creates a set of blobs generated by successive blurring of the image and collecting the most uniform objects (blobs). The blobs from different blurring levels are linked. For each blob, the number of survival steps over scales before disappearing or merging so called *a blob's lifetime* are calculated. The blob's lifetime implies the significance of a blob. Blobs with the largest lifetime are nominated as the OD candidates. Then a feature-based technique is applied to define the OD from the multiple candidates. The decision tree is constructed based on four features: blob size, blob compactness (roundness), blob entropy, and blob intensity. The blob entropy represents intensity variation of an image feature, in our study, to indicate the strong presence of blood vessels converging to the OD center. The entropy of a blob is defined as the probability distribution of a blob grey level in (3.4).

$$entropy = - \sum_i (p_i * \log_2 p_i) \quad (3.4)$$

where p_i is the i^{th} grey level the histogram obtained from a blob.

Our OD classification is performed using a decision tree which includes the above mentioned features along with the VT-feature. As stated in [68], the conventional SS decision tree in Figure 3.8 requires the compactness, entropy, and intensity for the OD classification. The corresponding thresholds are denoted by T_c , T_e , and T_i , respectively.

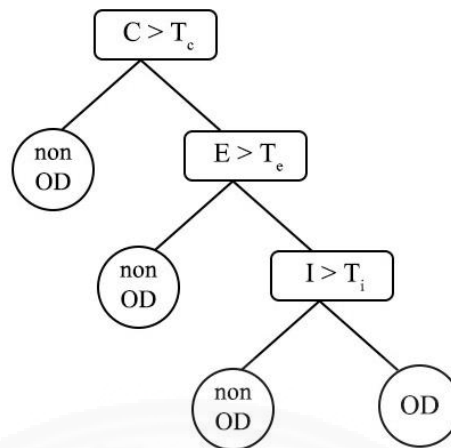


Figure 3.8: The conventional SS decision tree

The modified decision trees has been proposed by considering the productive VT-feature. The corresponding thresholds for the modified decision tree are the VT score, size, and compactness denoted by T_v , T_s , and T_c , respectively. The entropy and intensity denoted respectively by T_e and T_i have been excluded. The modified algorithm is called the scale space algorithm with the vessel transform (SSVT) and its illustration is shown in Figure 3.9. The corresponding features of each significant blobs over scales are utilized and taken into account of the decision tree for OD classification to return a selected blob as the OD.

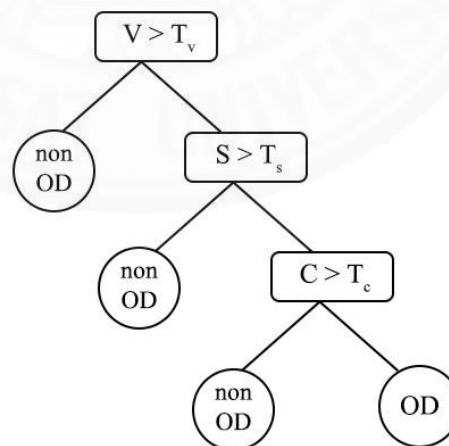


Figure 3.9: The SSVT decision tree

3.4 Advantage of the VT Approach

The main advantage of VT approach is that its concept is simple and easy to visual. The method does not require any OD feature, so it works well even in the images of which OD's appearance turns out insufficient feature information.

3.5 Disadvantages of the VT Approach

The VT mainly relies on a number of vessel collections. In some cases, the VT doesn't work well when the clustering algorithm returns less than three clusters which make it impossible to find convergence points. When such a case occurs, we simply discard the VT feature and apply the SS in its original version [68] to detect OD. Another disadvantage of this algorithm is that it requires as many as seven thresholds that are used for construction of the decision model for vessel selections. The last disadvantage, the VT approach depends heavily on the vessel segmentation algorithm and the clustering algorithm. Bad vessel segmentation algorithm and the clustering algorithm can cause a poor performance of the VT algorithm.

Chapter 4

Vessel Vector based Phase Portrait Analysis

In this chapter we present our second proposed approach namely *Vessel Vector based Phase Portrait Analysis* (VVPPA) to approximate the location of the OD. Figure 4.1 shows the overall process of the OD localization and segmentation using VVPPA and the modification of the SS. The structure of this chapter is organized as follows. Section 4.1 describes the vectors used in this approach. Section 4.2 describes the VVPPA algorithm to approximate the location of the OD. Section 4.3 describes how VVPPA is combined with the SS to obtain the OD region. The advantages and disadvantages of the VVPPA approach are discussed in section 4.4 and 4.5, respectively.

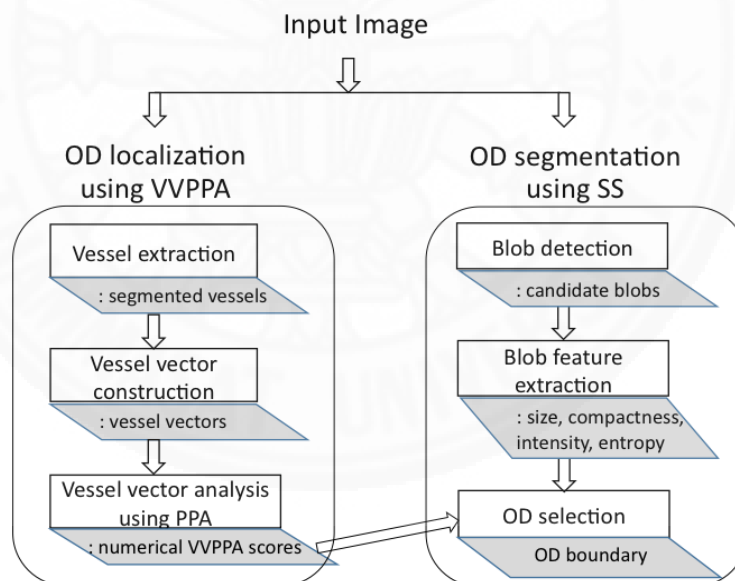


Figure 4.1: VVPPA combined with the scale-space segmentation

4.1 Vectors involved in this Approach

In this work, five types of vectors are prepared for VVPPA approach. The constructions of these vectors are described as follows.

4.1.1 Shifted Leading Vectors

To construct the shifted leading vectors, we considered *the bifurcation junctions* that associate with three vessel segments. The illustration of the considered vessels is shown in **Error! Reference source not found.**

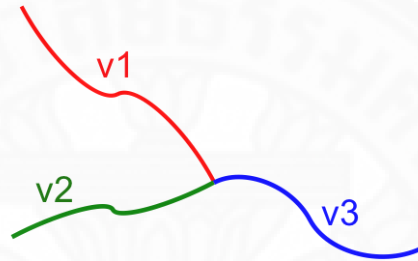


Figure 4.2: An example of bifurcation vessels

To construct main leading vectors obtained from bifurcations, for each junction, a circle centered at a junction with a radius r is drawn and the intersections of the circle with the vessel segments are marked. Vectors starting from a junction to the intersection points are then plotted and normalized to make three unit vectors called *the bifurcation vectors (BifV)*, as illustrated in Figure 4.3. From this point, to determine the main leading vectors from the BifV obtained in the previous process, the following features of the vessels are extracted: an opposite angle, a tortuosity, a thickness, and a contrast. The opposite angle of a vector is an angle between the other two vectors originated from the same bifurcation point. A tortuosity is a ratio of the distance to the displacement of two end points of the vessel segment. A thickness is an average width of the vessel segment considered only from the bifurcation point to the intersection point. A contrast is the difference of cumulative intensity between the vessel segments and surrounding background of the vessel segments from the bifurcation point to the intersection points. The values of tortuosity, thickness, and contrast are normalized with its maximum in the collection. For the case of degree,

the angle is normalized with 360. For all images in the collection, we find the BifV, collected their features, and used them for constructing a training model to classify a leading vessel vector. We divided BifV into two groups which are training and testing sets with proportion 70:30. Vectors in the training set are trained by providing answers of which vectors are leading and which are not along with the feature information. The rules are obtained from the training set and are applied to the testing set.

Once the leading vector is obtained, we take the vessel segment that the leading vector belongs to and then construct another unit vector that has the same direction as the leading vector which has the ending point at the non-bifurcation end point. This vector is called *shifted leading vectors* (SLV) illustrated in Figure 4.3. The SLV is used rather than the leading vectors because it is closer in location to OD much more than the ordinary leading vector.

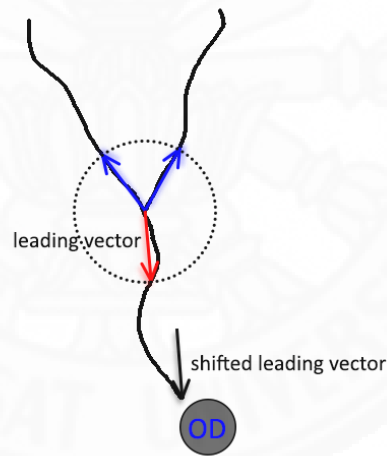


Figure 4.3: An illustration of a leading vector (red) and a shifted leading vector (black)

4.1.2 Sole Vessel Vectors

The sole vessels are also taken into our consideration as they are usually main vessels which contribute useful information about OD location. To generate sole vessel vectors (SVV), we selected sole vessels which were obtained well-defined crucial

information in length, thickness, and, contrast using a threshold selection technique similar to the VT. For each sole vessel, we randomly picked one end as a starting point and another end as an ending point, constructed a vector from these two points, and normalized it to get a unit vector. **Error! Reference source not found.** illustrates how the SSV is constructed. Remark that the directions of the sole vectors are going to be corrected in the VVPPA algorithm.

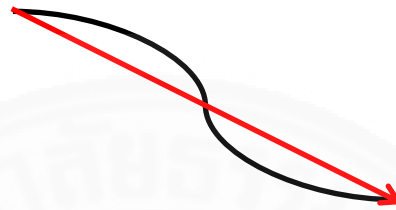


Figure 4.4: Illustration of how to construct a sole vessel vector

4.1.3 Mahfouz Vectors

The Mahfouz's probabilistic OD approximation proposed by Mahfouz et al. [47] is also taken into our consideration. Mahfouz's approach is based on the simple observation that the central retinal artery and vein emerge from the OD mainly in the vertical direction and then progressively branch into main horizontal vessels. From the vascular structure of the retina, a vertical bar with an image height and a proper width would always be dominated by vertical edges (vertical vessels) when centered at the OD. Thus, the *x-location* that yields the highest variation between vertical edge and horizontal edge is the vertical location of the OD. Once the vertical location is obtained, the *y-location* is determined by considering a square window with the length equals to the average diameter of the OD slid through this horizontal location to find a location that has the highest number of bright pixels.

Four unit vectors are created at the top and bottom of the retina edge and at the left and right of the retina edge, according to the vertical and horizontal directions obtained by the Mahfouz's approach. The directions of these four vectors are pointing toward inside of the retina image. Figure 4.5 shows OD *XY-location* using the Mahfouz's approach.

The Mahfouz's approach was experimentally proven to be fairly accurate for up to 92.6% [47]. It usually works well when the vessel structure is complete and shown high variation compared to surrounding background inside the OD. We thus employed the vectors derived from Mahfouz's approach as a part of our VVPPA algorithm. However, the Mahfouz's approach may not yield a good accuracy in images having poor quality. Figure 4.6 shows a case of anomalies on inhomogeneous illumination causing Mahfouz's vectors incorrectly locate OD. In this work we also aimed to enhance the accuracy of Mahfouz's approach by using the guiding directions of the vectors from the vessels as well as sub-vessels rather than the shape and orientation of the vascular network.

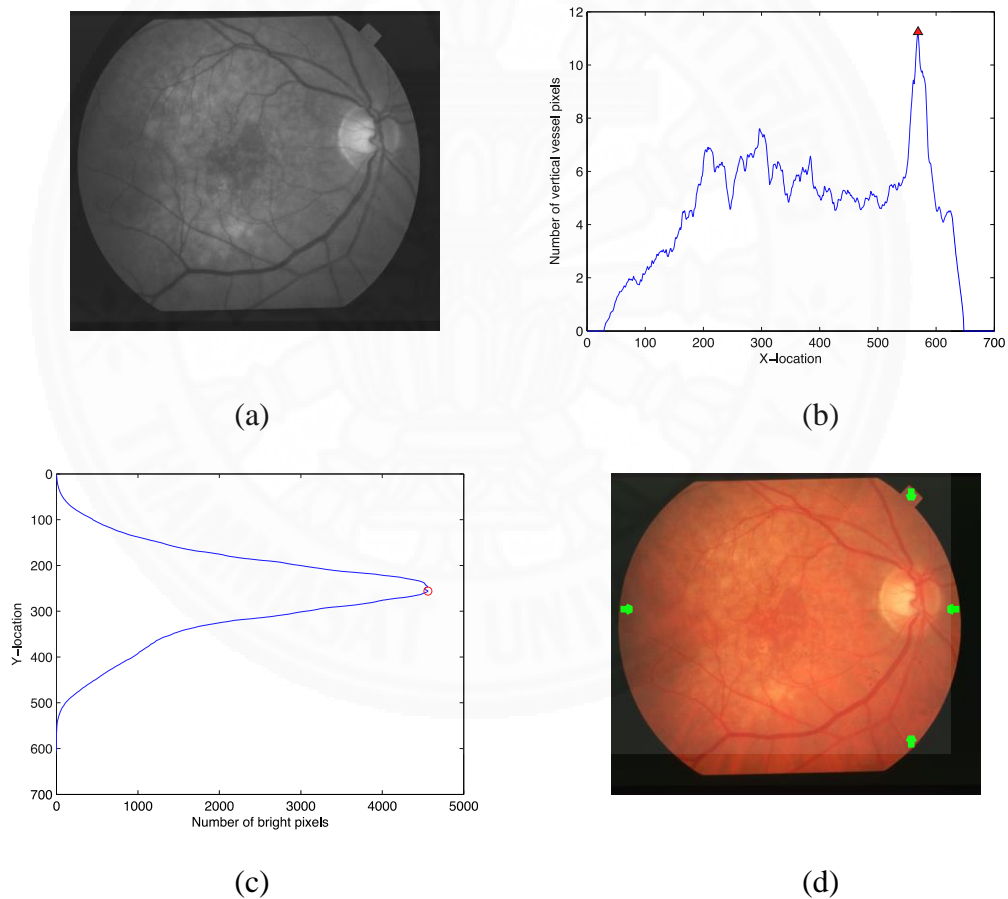


Figure 4.5: Illustration of how vectors from the probabilistic OD approach of Mahfouz are obtained. (a) original image (b) the greatest difference of number of pixels in vertical edge and horizontal edge. (c) y-location vs the maximum number of bright pixels in a reference square at x-location. (d) the Mahfouz vectors.

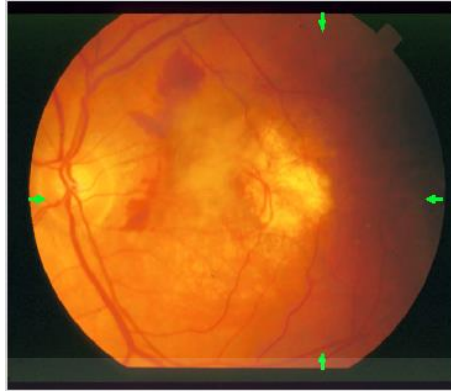


Figure 4.6: A false XY-location obtained the Mahfouz's approach

4.1.4 Bouncing Vectors

To control the convergence area of PPA to be within the retina, *bouncing vectors* (BV) are included. BV of a vector V are unit vectors starting at the edge of retinal image and pointing in the opposite direction to V . Figure 4.7 illustrates BV of two original vectors. In this work, the BV are applied onto the SLV, and the SVV.

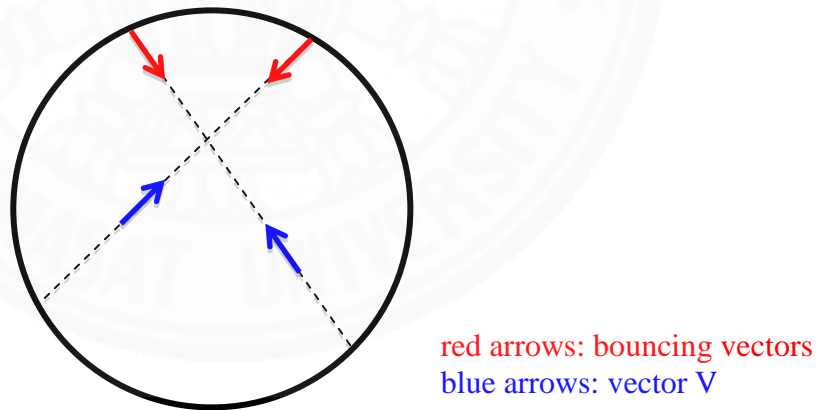


Figure 4.7: Illustration of bouncing vectors of two original vectors

4.1.5 Interpolation Vectors

At a grid point in the retina image, we interpolated a vector from its three nearest vectors obtained from the SLV, SVV, the Mahfouz's vector, and the bouncing vectors. The interpolation vectors are obtained by solving the system of linear equations described as follows. For each vector, suppose a triplet (a, b, c) represents the starting point (a, b) and its directional vector c . At a grid point (x, y) , we take three nearest vectors: $v_1 = (x_1, y_1, w_1)$, $v_2 = (x_2, y_2, w_2)$, and $v_3 = (x_3, y_3, w_3)$, and solve the following system of equations for vectors A, B , and C ,

$$\begin{aligned}w_1 &= Ax_1 + By_1 + C \\w_2 &= Ax_2 + By_2 + C \\w_3 &= Ax_3 + By_3 + C\end{aligned}\tag{4.1}$$

Then at a grid point (x, y) , its directional vector can simply be expressed as $w = Ax + By + C$.

4.2 Vessel Vector based PPA Algorithm

The vessel vector based PPA algorithm (VVPPA) requires all vectors except SVV described in section 4.1 and it returns the convergence location which is the centroid of PPA. The VVPPA algorithm is presented below.

In this algorithm, `Make_InterpolationVectors(V)` takes the collection of input vectors V to generate interpolation vectors, IV , at all grid points in the retina image. The function `Find_HighPPAScore_Region(IV)` finds and returns the convergent region ($CovReg$) of pixels having the high PPA scores obtained from PPA using the input collection of IV . As there can be many regions with high PPA scores, we select the convergent region by using the maximum likelihood estimation based on four features derived from the regions: the mean thickness of segmented vessels, contrast of segmented vessels compared to surrounding background, density of segmented vessels, and original PPA scores. `Find_Centroid(CovReg)` returns the centroid of the

convergence region $CovReg$. $Is_Pointing_outward(v,c)$ is another function that takes a vector v and a point c as inputs, returns true if v 's direction is toward c , otherwise false. To determine whether or not a vector v points toward a point c , we considered the end points of the vector, if the endpoint of v is closer to c than from its starting point to c , we stated that v was moving toward c . Figure 4.8 shows VVPPA steps in the algorithm.

Input:

SLV: A collection of shifted leading vectors

MV: A collection of Mahfouz vectors

BV: A collection of bouncing vectors

SV: the collection of sole vessels $\{sv_1, sv_2, \dots, sv_{|sv|}\}$

Output: centroid of PPA convergence region

VVPPA Algorithm:

$V = \{SLV, MV, BV\}$

$IV = \text{Make_InterpolationVectors}(V)$

#Determine the convergence region from PPA numerical scores

$CovReg = \text{Find_HighPPAScore_Region}(IV)$

$c = \text{Find_Centroid}(CovReg)$

for $i = 1:|SV|$

 #Validate the direction of sole vessel vectors

 if $Is_Pointing_outward(sv_i, c)$ is true

$sv_i = -sv_i$

 endif

 #Correct the location of convergence region

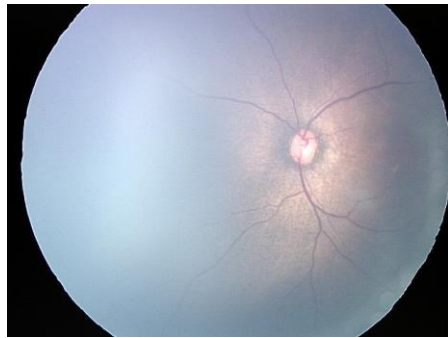
$V = V \cup sv_i$

$IV = \text{Make_InterpolationVectors}(V)$

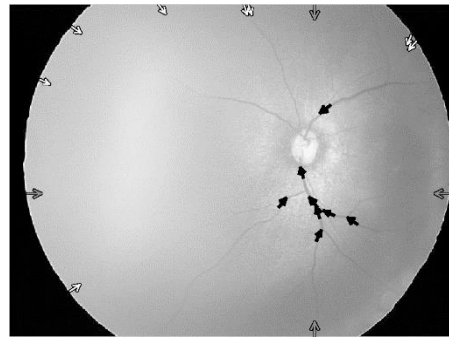
$CovReg = \text{Find_HighPPAScore_Region}(IV)$

$c = \text{Find_Centroid}(CovReg)$

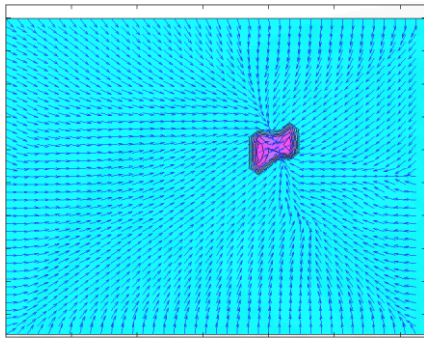
endfor



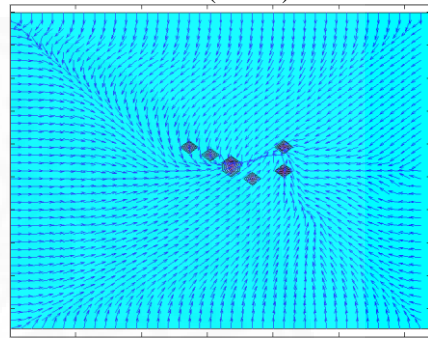
(a) Original image



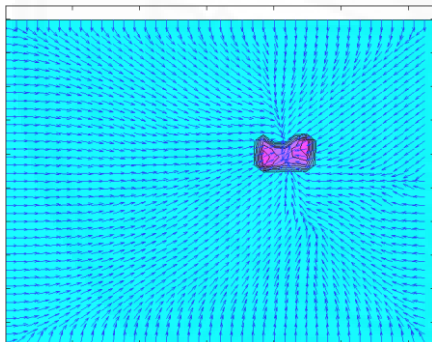
(b) SLVs (black), MVs (gray), and BV (white)



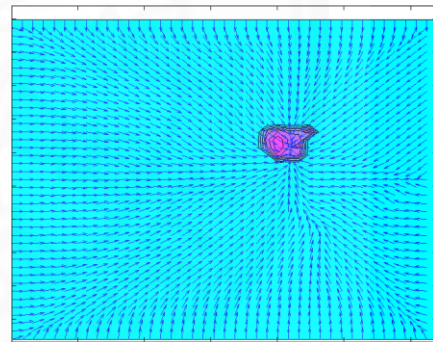
(c) IVs and the initial CovReg



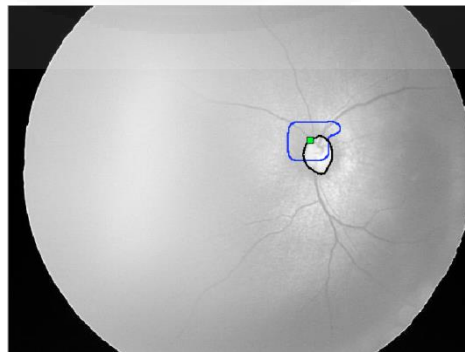
(d) IVs and CovReg after including the 1st sole vessel vector



(e) IVs and CovReg after including the 2nd sole vessel vector



(f) IVs and CovReg after including the 3rd sole vessel vector



(g) Centroid (green rectangle) of CovReg boundary (blue line) and the ground truth boundary (black line)

Figure 4.8: Illustration of steps in VVPPA algorithm

4.3 Scale Space Algorithm with VVPPA for OD Segmentation

Similar to SSVT defined in the earlier chapter, we employed our new information PPA score obtained from VVPPA with existing blob features: size, compactness (roundness), entropy, and intensity to construct a decision model for OD selection. Intensity variation so called blob entropy, in our study, represents an alternative image feature to indicate the strong presence of blood vessels converging to the OD center. The corresponding decision trees requires thresholds the PPA score, size, entropy, and compactness denoted by T_p , T_s , T_e , and T_c , respectively, for the SSVVPPA decision tree. The intensity denoted by T_i has been excluded after pruning the SSVVPPA decision tree. The modified OD segmentation algorithm is called scale space algorithm with vessel vector based phase portrait analysis (SSVVPPA) and its illustration is shown in Figure 4.9. The corresponding features of the significant blobs over scales are utilized and taken into account of the OD classification model to return a selected blob as the OD.

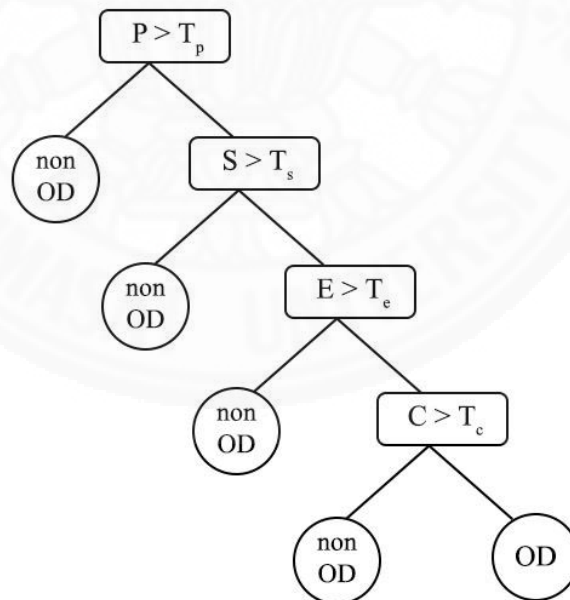


Figure 4.9: The SSVVPPA decision tree

Instead of using standard features such as size, compactness, entropy, and intensity as in the work of Duangate et al. [68] to segment the OD boundary using SS, SSVVPPA uses a PPA score obtained from VVPPA detection algorithm as an

additional feature to the existing features to enhance the performance of the SS OD segmentation algorithm. Figure 4.10 demonstrates the OD rims obtained from SS and SSVVPPA compared with ground truths. The results show that SSVVPPA yields a more accurate OD region than SS.

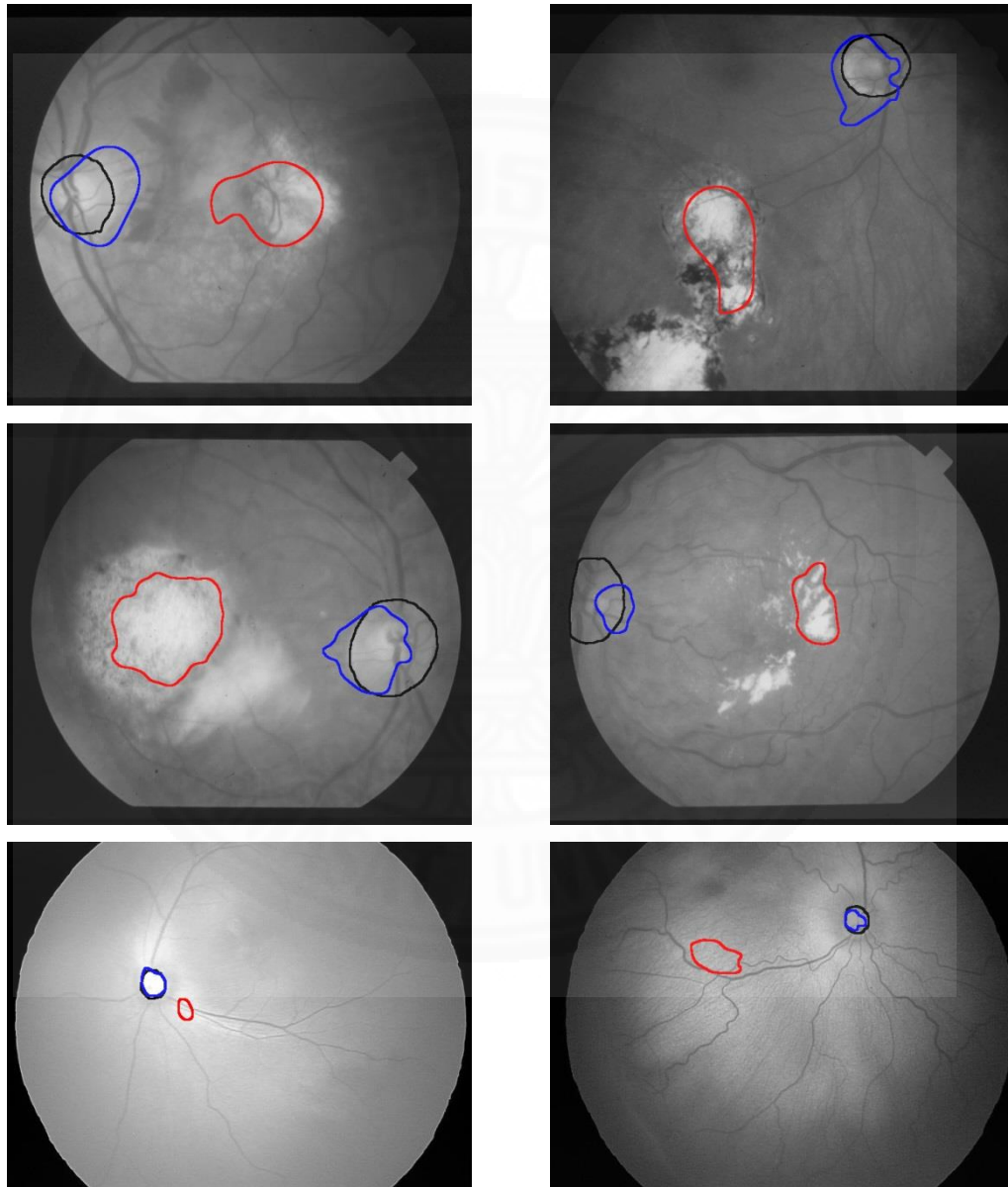


Figure 4.10: Examples of OD rims obtained from SS (red solid) and SSVVPPA (blue solid) compared with ground truths (black solid) of six images

4.4 Advantages of the VVPPA Approach

The VVPPA relies on sufficient vessel junctions and branch points inside the retinal image to construct vessel vectors beyond finding the convergent OD regions using PPA. The approach is effective and accurate on OD detection even blood vessels are obscured by the pathological regions and the pathological regions present the similar features of the OD. This is because the entire vascular structure forms the meaningful branches and adequate vessel junctions. The additional vectors are also generated to bind the vector flow particularly inside the retina edges and strengthen the vector trajectory pattern of the convergence. Furthermore, this approach is robust to rotational variation when the OD position is roughly shifted away from the center of retina.

4.5 Disadvantages of the VVPPA Approach

The VVPPA depends on the number of vessel junctions and branches in the image. For some images that have very few vessel junctions and branch points, VVPPA may yields incorrect results. Figure 4.11 below shows examples of such a case.

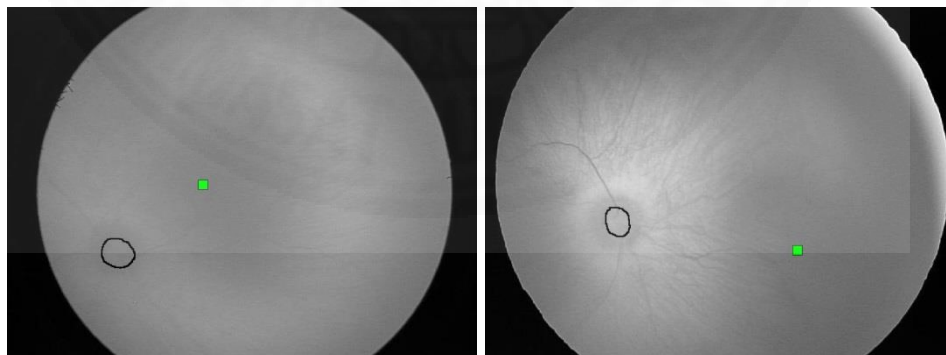


Figure 4.11: Examples of images that VVPPA fails due to insufficient information from the vessels. Green rectangle shows OD location obtained from VVPPA.

For such a case, the user needs to use other approaches which depend on OD features instead. Another limitation is that VVPPA depends heavily on the vessel segmentation algorithm. When the vessel segmentation algorithm is poor, it may result in low accuracy.



Chapter 5

Hybrid Approach for OD Detection

In this chapter, our third approach for OD detection is described. This approach basically aims to carry out the best accuracy of the other two proposed approaches which VT and VVPPA are combined. We name this approach the *Hybrid Approach* (HA). The overall process of the OD localization and segmentation using HA is illustrated in Figure 5.1. The algorithm is provided in section 5.1 including advantages and disadvantages of the approach are stated in section 5.2 and 5.3, respectively.

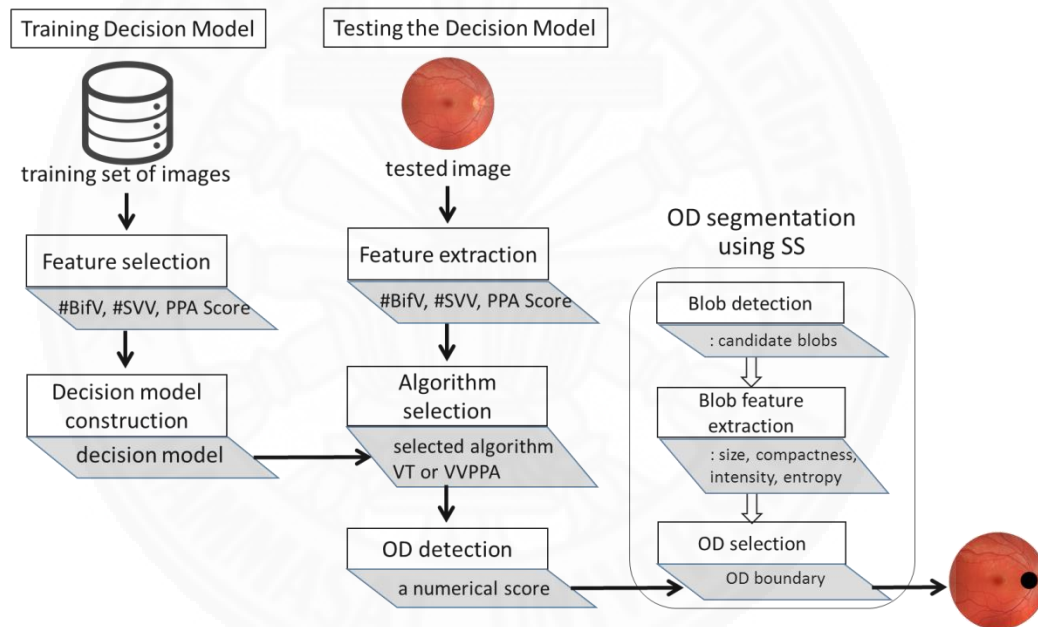


Figure 5.1: The OD localization and segmentation using HA

5.1 Hybrid Approach

To localize the OD, the HA creates the decision model for selecting an appropriate approach between VT and VVPPA to be employed in each particular case. The selected features mainly obtained from VVPPA approach. These features are the number of BifV, the number of SVV, and PPA score.

The HA can be summarized into an algorithm as follows.

Algorithm Hybrid Approach(C, I):

Input:

C = A collection of images of size N

I = An image in C that the user would like to determine the OD location

T = input training set of images of size N_t where $N_t < N$

$F(T) = \{F_1(T), F_2(T) \dots, F_M(T)\}$ where $F_i(T)$ is the i^{th} feature vector of T. The component of vector $F_i(T)$ is the feature values of the corresponding image in T

ANS(T) = a binary answer set vector (0 for VT and 1 for VVPPA) of T of size N_t

Output:

algV = a binary vector contains answers

Hybrid Approach Algorithm:

% generate the decision model

DModel= Calculate_Decision_Model(F(T), ANS(T))

% Determine the answers for the input image

FI = $\{F_1(I), F_2(I) \dots, F_M(I)\}$

algV = Select_Algorithm(DModel, FI)

The Calculate_Decision_Model(F(T), ANS(T)) generates the decision model using the feature vector F(T) and the solution from the training set ANS(T). The function Select_Algorithm(DModel, FI) returns the algorithm that should be used for the image I using the DModel obtained from the Calculate_Decision_Model(F(T), ANS(T)) and FI is the feature vector (1 X M dimension) of I.

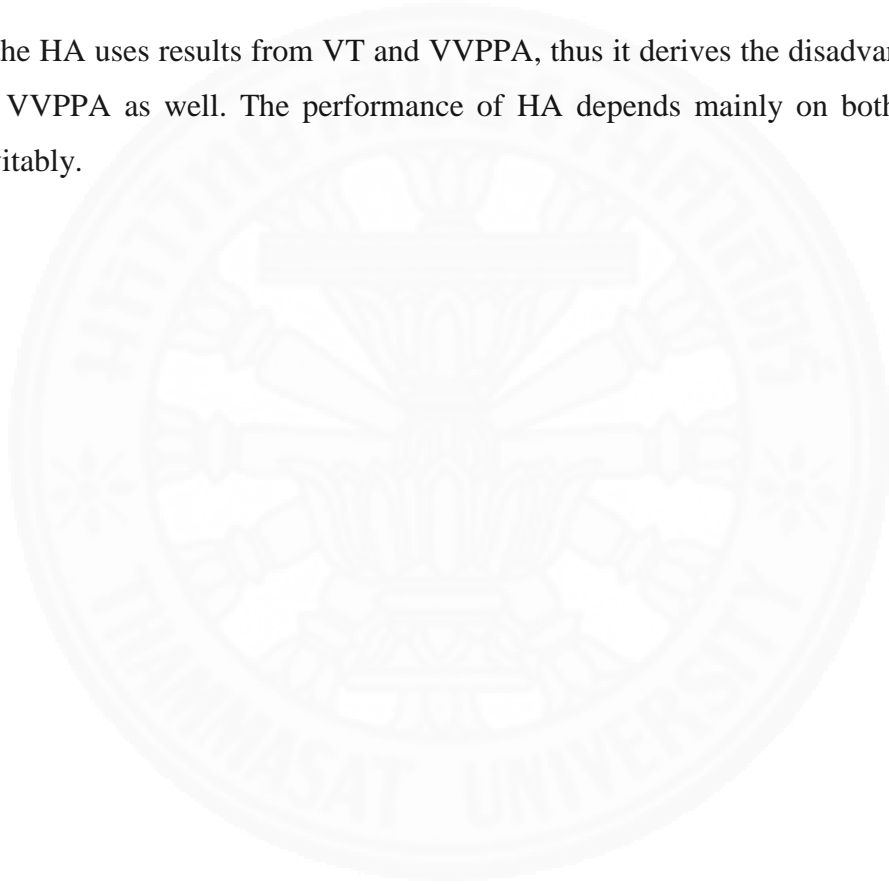
For OD segmentation, either SSVT or SSVVPPA is selected according to the localization algorithm (VT and VVPPA) resulted from the hybrid algorithm namely SSHA. The choices of features and the decision models used in the experiments are provided in the experimental settings. The corresponding evaluation results and discussion are provided in Chapter 7.

5.2 Advantages of the HA

The HA takes good results from both approaches, so its performance is usually better than VT and VVPPA. The HA can reduce the computational time twice instead of using individual approach.

5.3 Disadvantages of the HA

As the HA uses results from VT and VVPPA, thus it derives the disadvantages of VT and VVPPA as well. The performance of HA depends mainly on both approaches inevitably.



Chapter 6

Experimental Setup and Evaluation Schemes

This chapter describes the image collections as well as the evaluation schemes used in our experiments. The details about the retinal fundus image collections used in the experiments, the vessel segmentation algorithm, the ground truth data, the experimental setup, and the evaluation schemes are described in sections 6.1, 6.2, 6.3, 6.4, and 6.5, respectively.

6.1 Retinal Fundus Image Collections

For our experiments, we used two collections of the retinal fundus images: the STructured Analysis of the REtina (STARE) [72] which is a standard database available on the internet. The fundus photographs from STARE were captured by a TopCon TRV-50 fundus camera with 35 degree field of view. Each image was digitized to create a 605 x 700 pixels at 24 bits per pixel. Another collection is a dataset originally collected to detect the signs of retinopathy of prematurity (ROP) by Dr. Sarah Barman with Kingston University of UK. All digital images from ROP were taken from patients with non-dilated pupils using a KOWA-7 non-mydratic retinal fundus camera with a 45 degree field of view. The images were stored in JPEG format 640 x 480 pixels at 24 bits per pixel.

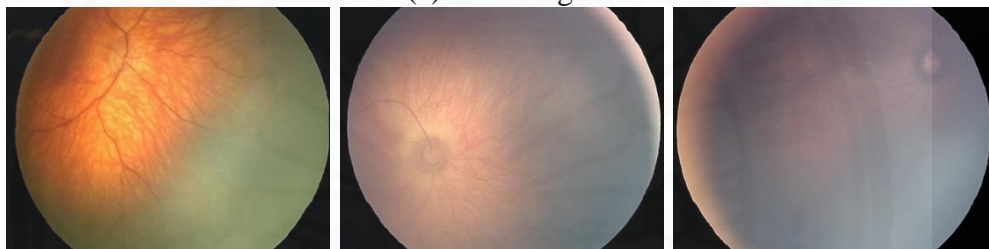
As our approaches proposed to improve OD localization and segmentation emphasized on imperfect retinal images, so in this work we classify images into two categories. The bright, elliptic, and clear edge images of the ODs were classified visually as “fair”, the rest is considered ‘poor’. The number of the retinal images grouped by image quality and their average diameters of ODs’ ground truth are shown in Table 6.1. The examples of “fair” and “poor” retinal fundus images are displayed in Figure 6.1 and Figure 6.2 for ROP and STARE collections, respectively.

Table 6.1: Classification of the images into fair and poor

Collections	Image quality	Number of images	Average diameter of ODs' ground truth (pixels)
ROP	Fair	60	49.03
	Poor	31	46.73
STARE	Fair	31	102.16
	Poor	50	105.61

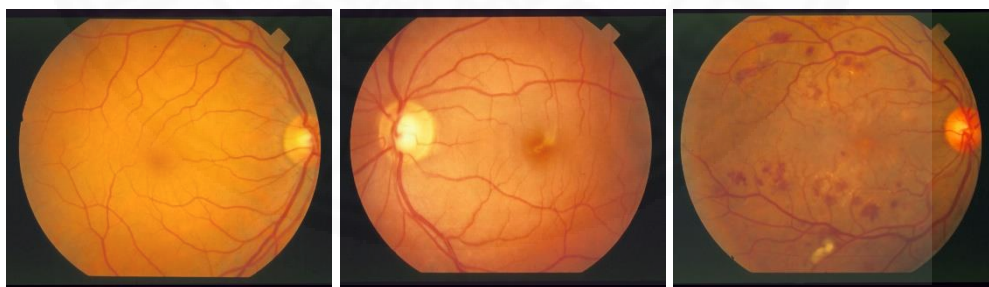


(a) Fair images



(b) Poor images

Figure 6.1: Examples of “fair” and “poor” images from ROP



(a) Fair images



(b) Poor images

Figure 6.2: Examples of “fair” and “poor” images from STARE

6.2 Retina Vessel Extraction Software

The vessel extraction algorithm namely *Automated Retinal Image Analyser (ARIA)* [73][74] developed by the Center for Vision and Vascular Science of Queen's University of Belfast were applied to both image collections. The software can be downloaded from <http://sourceforge.net/p/aria-vessels>. The method is based on thresholding of wavelet coefficients over different spatial scales and vessel location refinement using a centerline spline fitting to point out the vessel edges in the image profile. The method is unsupervised and does not require masks or filters since they often must be tailored for a particular type or resolution of the image and require modifications to be applied to others. As opposed to that the choice of wavelet levels and thresholds does not need to be changed for similar images, following [73][74], we set the wavelet coefficient threshold to identify the lowest 20% of coefficients as vessels. Although this typically produces an oversegmented image, small isolated objects and holes inside the vessels can be easily removed and filled by the post-processing, morphological operations. Figure 6.3 shows the example of final extracted retinal vessels where the outer pink lines are the vessel edges and each segment is labeled by the numbering system.

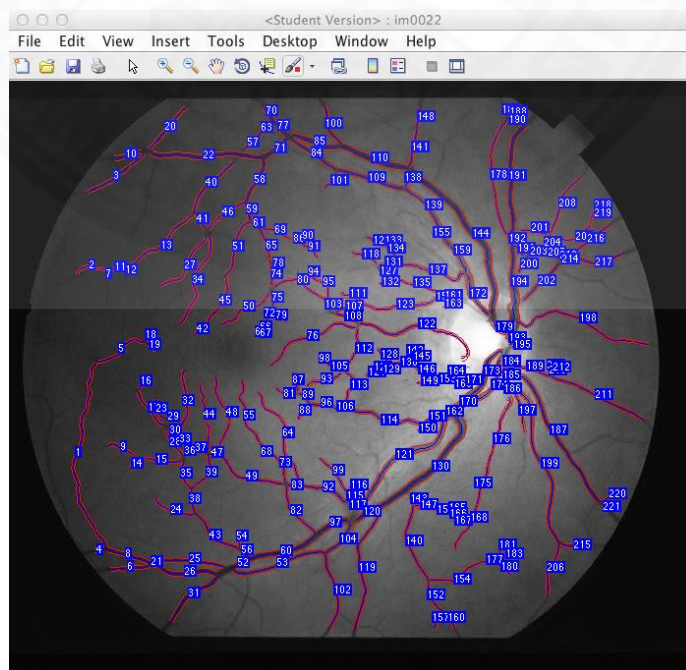


Figure 6.3: Extracted retinal vessels using ARIA

6.3 Ground Truth

To evaluate the numerical experiment of the proposed method, hand-drawn ground truth (GT) images were obtained from human experts. To minimize human expert discrimination, the ground truth was obtained from three ophthalmologists from Thammasat University Hospital, Thailand. Each ophthalmologist was asked to hand-draw the OD contours on each retina image from two collections three times. The variability of the experts is taken into account in term of reliability. The voting overlapping score is defined as the ratio of an area in the GT images that at least two GTs agree on a part of OD to the area obtained from the union of the three GT contours. The inter-observer variability is determined as the score from the three GT contours obtained by three experts. The inter-observer variability values of the experts are 0.86 and 0.91 for the ROP and STARE collections, respectively. Figure 6.4 shows the area where at least two experts agree. The intra-observer variability is determined as the score from the three GT contours obtained by the same expert. The intra-observer variabilities of each expert are 0.92 and 0.93 on average for the ROP and STARE collections, respectively.

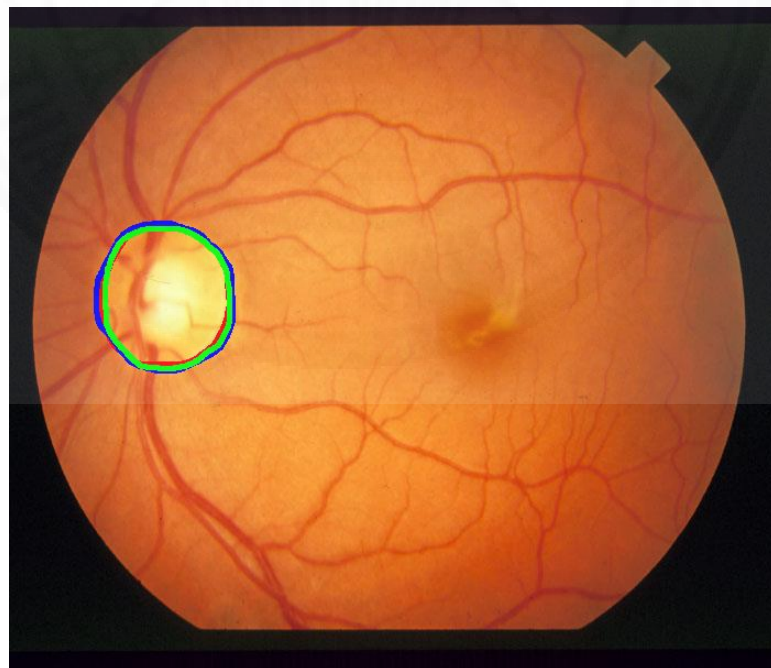


Figure 6.4: Illustration of finding the voting overlapping score from GT contours (blue, red, and green circles are given GT contours obtained by the first, second, and third experts, respectively)

6.4 Settings

6.4.1 For VT Approach

Our two collections of the test images have been obtained from different devices with different lighting conditions. Therefore, they require different sets of thresholds which are obtained by the quadratic regression. We trained the method using the classic 70-30% ratio between the training and the testing data. The thresholds used for vessel selection of the vessel clustering algorithm were obtained by using quadratic regression on the training set of each collection. Following thresholds are computed: T_l - the minimal acceptable length of the vessel for a particular image (shorter vessels will be eliminated), T_t - the minimal acceptable thickness, T_f - the maximum acceptable intensity of the vessel relative to the background, T_d - the maximum distance between the clusters which can be merged into a new cluster, T_L - the minimum acceptable size of the cluster, T_Ω and T_{VT} the thresholds used in the convergence test are required. Figure 3.4 and Figure 3.5 in Chapter 3 illustrate the threshold selections applied to the ROP and the STARE set, respectively.

6.4.2 For VVPPA Approach

To obtain the decision model of leading vector classification, we employed Gaussian Radial Basis Function kernel (RBF) of Support Vector Machine (SVM) applied onto the training set of collection of vessel features. The decision models for leading vector classification are shown in Figure 6.5 and Figure 6.6 where red and blue markers represent the feature values of the leading and non-leading vectors, respectively. The X, Y, Z-axes represents the normalized values of 3 features-opposite angle, the tortuosity, and the intensity, respectively. The black line indicates the decision boundary of the classifications after applying feature selection method. Accuracies of classification models on testing set are 96.61% and 94.11% for ROP and STARE, respectively.

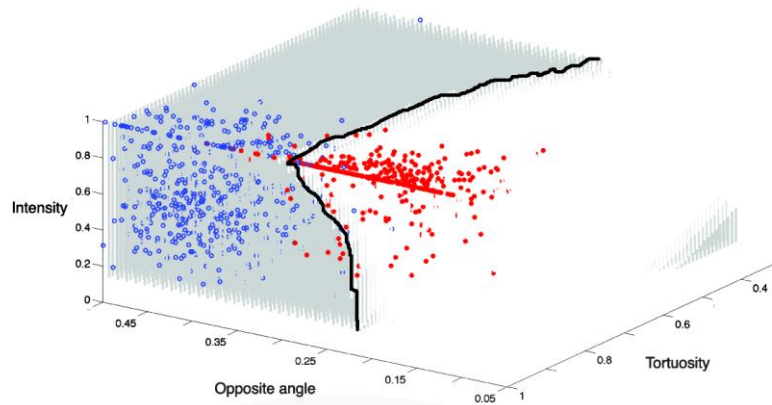


Figure 6.5: Decision model of leading vector classification for ROP, red – data of the leading vectors and blue – data of the nonleading vectors

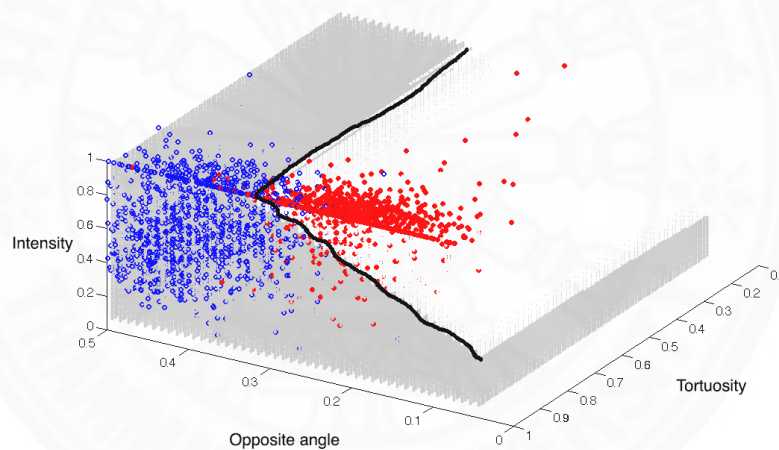


Figure 6.6: Decision model of leading vector classification for STARE, red – data of the leading vectors and blue – data of the nonleading vectors

6.4.3 For SSVT Approach

To identify OD blob using SS, the decision tree as shown in Figure 6.7 is applied on to set of blobs' features: blob size (s), compactness (c), and VT-score (v).

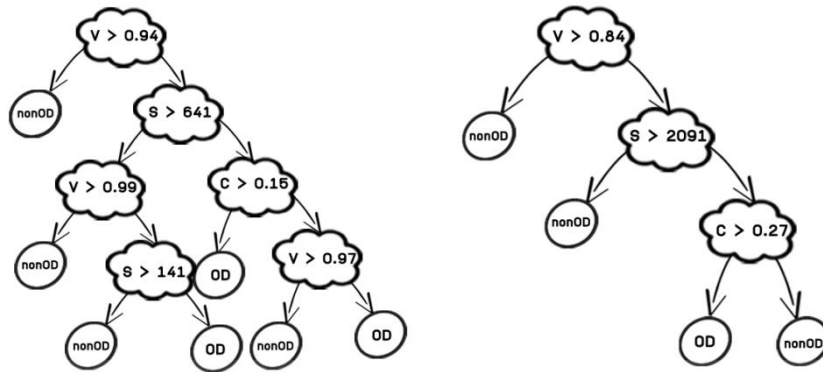


Figure 6.7: SSVT decision trees for test collections: (left) ROP collection and (right) STARE collection

6.4.4 For SSVVPPA Approach

Seventy-percent of all feature records are then trained to define the competent decision tree model and the rest of feature records is for the testing set. The corresponding decision model requires thresholds for the PPA score, size, entropy, compactness, and intensity denoted by p , s , e , c , and i , respectively as shown in Figure 6.8. The intensity has been excluded. The modified algorithm is called the space scale algorithm with the vessel vector based phase portrait analysis (SSVVPPA). The following decision tree is used for classification of OD and nonOD.

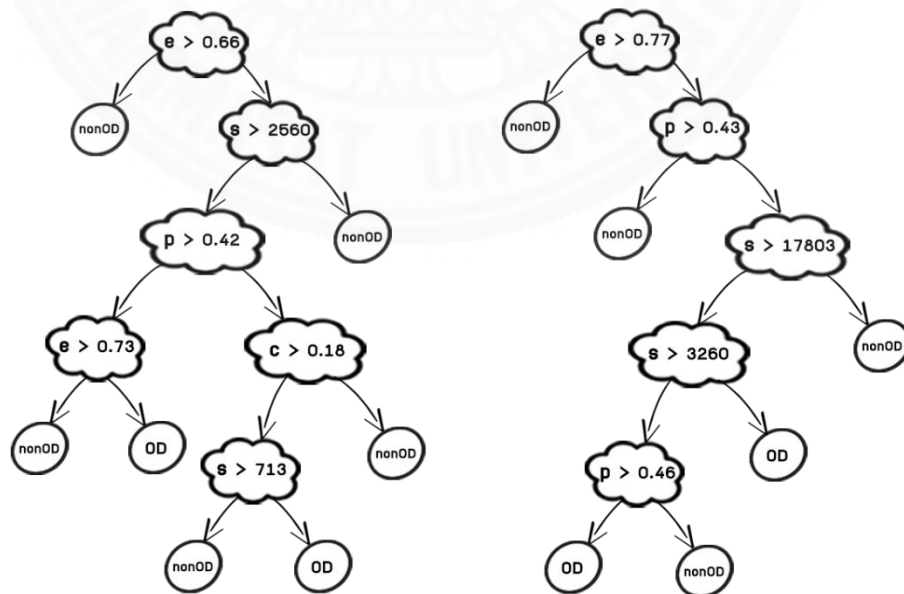


Figure 6.8: SSVVPPA decision trees for test collections: (left) ROP collection and (right) STARE collection

6.4.5 For Hybrid Approach

The both image collections were trained to obtain a rule for OD localization. The features of vectors derived from VVPPA was considered mainly as the basis model rather than those of VT due to the fact that features obtained from VT take considerably long computational time.

The feature selection for training set mainly relies on VVPPA approach which are the number of BifV, the number of SVV, and PPA score obtained from VVPPA. One decision system model applied for both ROP and STARE collections is represented in Figure 6.9.

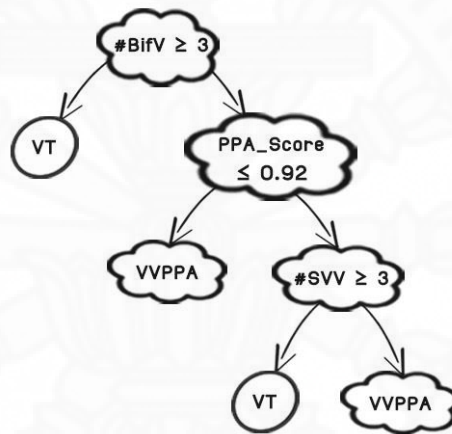


Figure 6.9: Decision system model of hybrid approach for OD localization

6.5 Evaluation

Two evaluations were used for OD localization and segmentation. The evaluation scheme for OD localization is as follows. If the approximate OD location is contained entirely inside the ground truth's contour, it is considered a correct location of the OD. The ratio of the correct cases to the total number of images yields the average accuracy. We evaluated the performance of all methods for OD localization by average accuracy.

We evaluated the performance of the OD segmentation using two standard schemes: sensitivity and positive predictive value (PPV). The first one reveals the correctness while the second one reflects completeness of the obtained solution. The sensitivity is defined to be the ratio of the number of pixels detected correctly as the OD to the total number of pixels detected as the OD. The PPV is the ratio of number of pixels detected correctly as the OD to the total number of pixels of the OD from the ground truth. These two measurements can be calculated based on four values, namely:

- The true positive (TP) rate: the number of OD pixels correctly detected
- The false positive (FP) rate: the number of non-OD pixels wrongly detected as OD pixels
- The false negative (FN) rate: the number of OD pixels not detected
- The true negative (TN) rate: the number of non-OD pixels correctly identified as non-OD pixels

and its demonstration are defined in Figure 6.10.

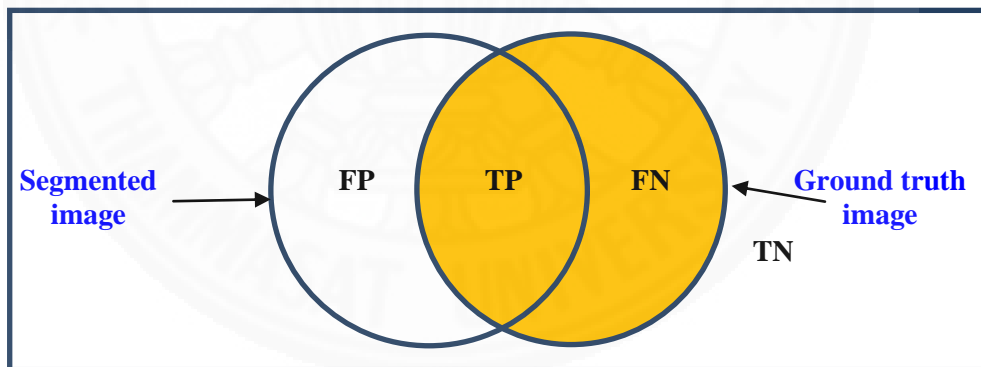


Figure 6.10: The four values demonstration as set

6.6 Experiment

We compared our proposed OD localization approaches: VT, VVPPA, and HA with the Lu's circular transformation method (CTM) [44] and Fuzzy Convergence (FC) method [4]. To evaluate the efficiency of OD localization, the proposed approaches

were applied on one hundred seventy-two retinal images from the ROP and STARE collections.

Three variations of the SS which included information of scores VT, VVPPA, and HA, so-called respectively, SSVT, SSVVPPA, and SSHA are also tested against the SS without these information and also against the CTM OD segmentation algorithms. The results of the experiments are provided in the next chapter.



Chapter 7

Experimental Results and Discussion

In this chapter, we report and analyze results of our proposed approaches to the collections of the retinal images. For OD localization, we compared results of our three proposed approaches (VT, VVPPA, and HA) to find an approximate location of the OD against the Fuzzy Convergence (FC) method [4] and a recent modification of the circular transform proposed in [44] (LU). For OD segmentation, we compared the results of those approaches combined with the SS (SSVT, SSVPPA, SSHA) against the SS. The numerical results of the OD localization and segmentation approaches are provided in section 7.1 and 7.2, respectively. The discussions about the results are given in section 7.3.

7.1 Numerical Experiments of the Approaches in Locating the OD

Figure 7.1 shows samples of qualitative results of five approaches applied to eight selected images. Our proposed approaches: VT, VVPPA, and HA generally perform better than the existing methods (FC and CTM). The numerical accuracies of 5 different OD localization approaches for all images classified by the fair and poor qualities are shown in Table 7.1.

The results shows that in terms of accuracy, the proposed approaches VT, VVPPA, and HA noticeably outperform FC by 6.22, 8.84, and 9.84 in absolute improvement respectively for both fair and poor sets on STARE database. Both VVPPA and HA reach the same highest accuracy as CTM of 100% for the fair case of STARE collection. As we assert that our proposed approaches work better than CTM on both test collections, the absolute improvement shows outperformance in accuracy for fair quality images by 1.72, 5.84, 5.84, and for poor quality images by 14.12, 8.67, 16.12 through VT, VVPPA, and HA approaches, respectively.

For the poor quality images of the STARE collection, VT and VVPPA slightly underperform CTM respectively by 4.00 and 2.00 whereas HA has the equivalent performance to CTM. When compared to FC, the accuracy results show slightly

higher number of absolute improvement by 6.00, 8.00, and 10.00 using VT, VVPPA, and HA, respectively. For the ROP collection, since there is no information about the accuracy of FC, we cannot compare the performances of our proposed approaches with it. For the poor quality images of the ROP collection, VT, VVPPA, and HA outperform CTM considerably on absolute improvement by 32.25, 19.35, and 32.25, respectively.

For the fair quality images of STARE collection, VT shows degradation against CTM by 3.23 whereas VVPPA and HA are shown equivalence in numerical results. In contrast to the results obtained from the ROP collection, the absolute improvement are reported the performances against CTM by 6.67, 11.67, and 11.67 for VT, VVPPA, and HA, respectively. VT, VVPPA, and HA are reported better performances on STARE fair quality images against FC by 6.45, 9.68, and 9.68 of absolute improvement respectively. Remark that the comparisons of our approaches against FC on ROP are unable to verify due to the unavailable information.

VVPPA generally works better than VT on STARE, and fair set of ROP. VT outperforms VVPPA only for the poor quality images of ROP's collection. As the HA selectively uses results of VT and VVPPA, it improves the accuracy, the highest average accuracy of up to 98.00 for poor images and as high as 100.00 for fair images.

For all image collection, the absolute improvements of VT, VVPPA, and HA show noticeably better than CTM by 14.12, 8.67, and 16.12, respectively for the poor sets, and 1.72, 5.84, and 5.84, respectively for the fair sets.

Furthermore, all three proposed approaches (VT, VVPPA, and HA) significantly outperform CTM with the absolute improvement 19.46, 15.51, and 21.96, respectively on the ROP collection. The numerical experiments show the degradation 3.62 and 1.00 through VT and VVPPA, respectively while HA works equally against CTM for the STARE collection.

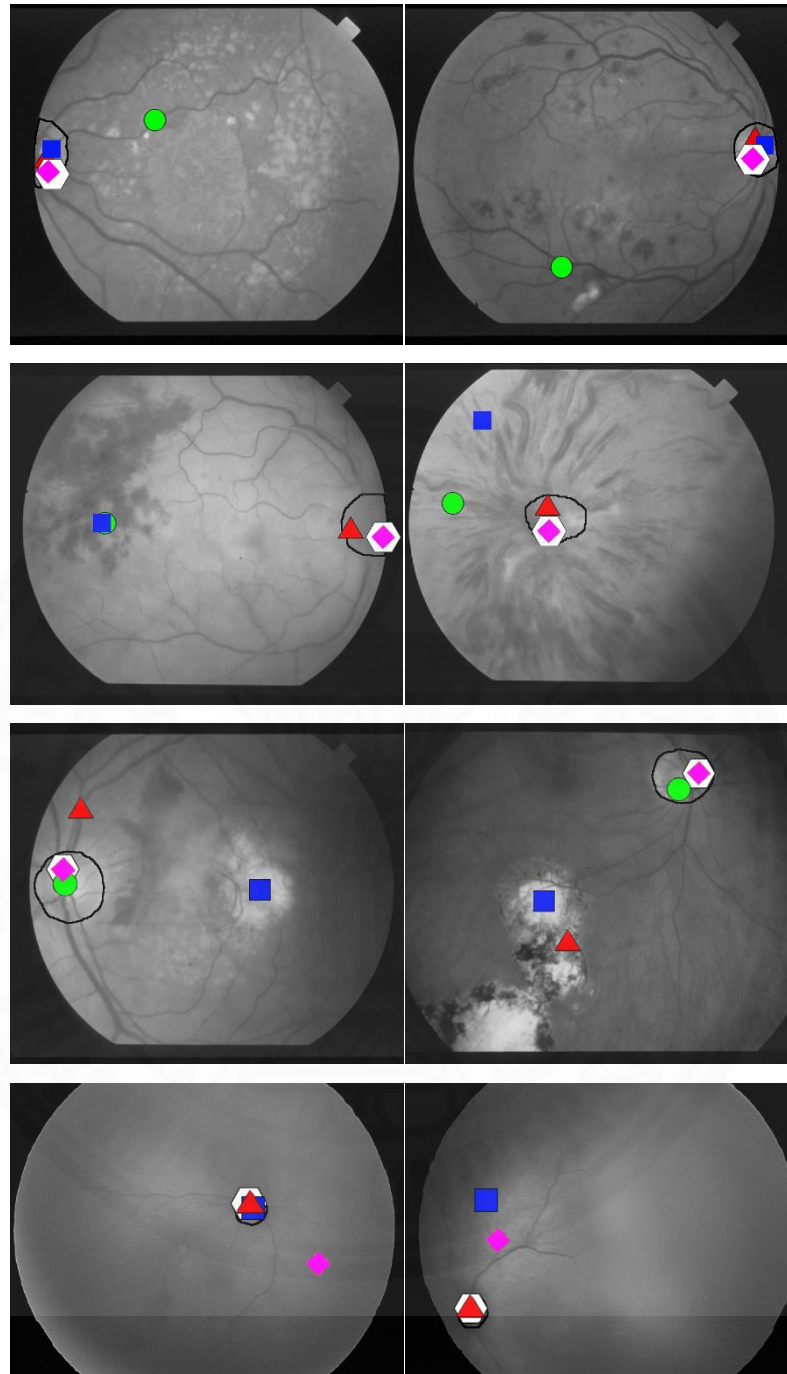


Figure 7.1: Examples of OD locations obtained from different approaches on eight images, Ground truth –black solid line, FC – green circle, CTM – blue square, VT – red triangle, VVPPA – pink diamond, and HA –white hexagon.

Table 7.1: Accuracy of the OD location using FC, CTM, VT, VVPPA, and HA

Collections	ROP		STARE		Overall average for ROP	Overall average for STARE	Overall average for Fair	Overall average for Poor
	Fair	Poor	Fair	Poor				
FC	N/A	N/A	90.32	88.00	N/A	89.16	N/A	N/A
CTM	88.33	64.52	100.00	98.00	76.42	99.00	94.16	81.26
VT	95.00	96.77	96.77	94.00	95.88	95.38	95.88	95.38
VVPPA	100.00	83.87	100.00	96.00	91.93	98.00	100	89.93
HA	100.00	96.77	100.00	98.00	98.38	99.00	100	97.38

7.2 Numerical Experiments of the Approaches in Detecting the OD Region

In this section, we provide the results of the OD segmentation from our OD localization approaches combined with the Scale Space (SS) algorithm proposed by Duanggate et al. [68]. SSVT, SSVVPPA, and SSHA are compared with the existing conventional OD segmentation approaches: CTM and SS.

The numerical results between the comparison-based methods and the proposed methods of two major evaluations: sensitivity and positive predictive value (PPV) are presented in Table 7.2. The bold values represent the best result in a particular category.

Table 7.2: Accuracy of the OD segmentation using CTM, SS, SSVT, SSVVPPA, and SSHA

Evaluation	Methods	ROP		STARE		Average on all collection	Average for Fair sets	Average for Poor sets
		Fair	Poor	Fair	Poor			
Average Sensitivity	CTM	74.29	61.28	72.59	41.23	62.35	73.44	51.25
	SS	80.39	45.51	57.95	43.27	62.20	69.17	44.39
	SSVT	82.47	58.18	62.40	45.76	64.26	72.43	51.97
	SSVVPPA	82.47	55.39	64.84	47.91	62.65	73.65	51.65
	SSHA	82.47	58.18	64.84	47.93	63.35	73.65	53.05
Average PPV	CTM	66.42	46.39	84.66	69.89	66.84	75.54	58.14
	SS	86.08	53.01	67.09	59.18	66.34	76.58	56.09
	SSVT	87.41	83.85	74.14	74.59	80.00	80.77	79.22
	SSVVPPA	87.41	74.71	76.12	72.39	77.66	81.76	73.55
	SSHA	87.41	83.85	76.12	74.39	80.44	81.76	79.12

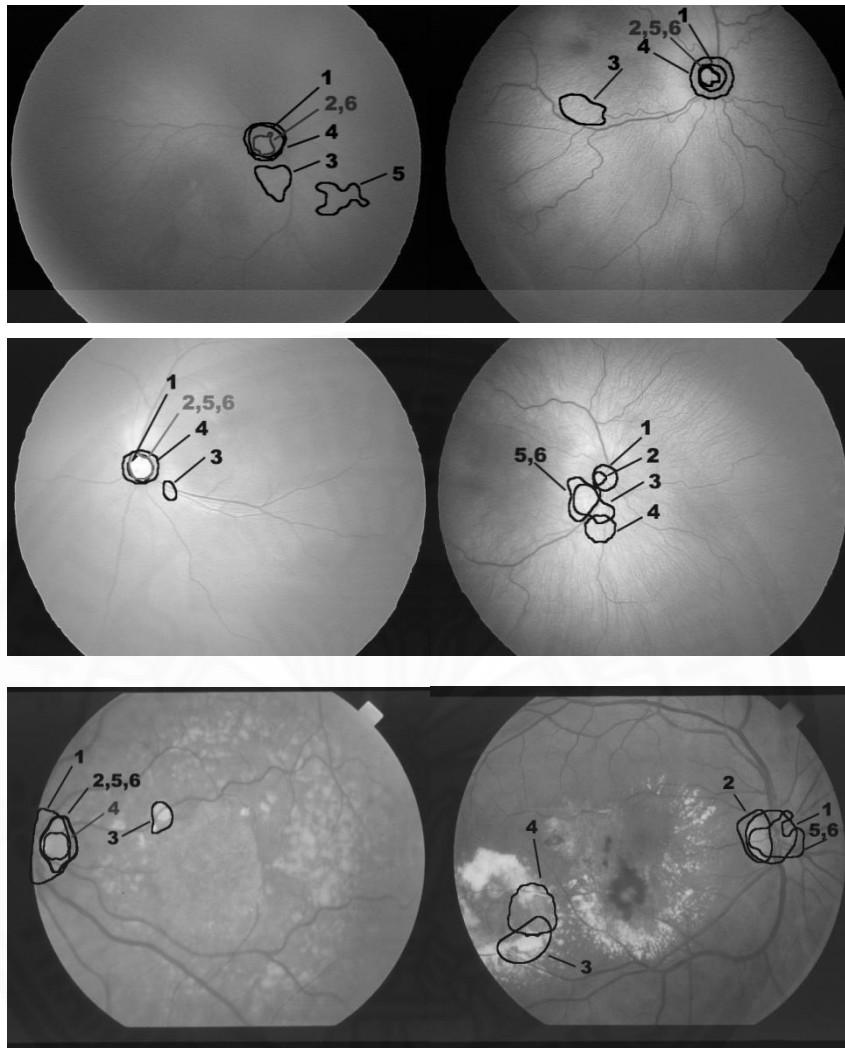


Figure 7.2: Examples of OD regions: 1-ground truth, 2-SSVT, 3-SS, 4-CTM, and 5-SSVPPA, or 6-SSHA

From the results in the Table 7.2, our proposed approaches perform better than the comparison-based methods for fair quality set of ROP collection, for both sensitivity and PPV evaluation schemes. The absolute improvements of SSVT, SSVPPA, and SSHA over CTM are all equal 8.18 for sensitivity and all equal 20.99 for PPV. In comparison, the absolute improvements of SSVT, SSVPPA, and SSHA over SS's are all the same 2.08 for sensitivity and all the same 1.33 for PPV.

It has been shown that the sensitivity in ROP poor collection of SSVT, SSVPPA, and SSHA against CTM shows degradation slightly in OD detecting by 3.1, 5.89, and

3.1, respectively. While SSVT, SSVVPPA, and SSHA noticeably outperform SS with the absolute improvement 12.67, 9.88, and 12.67, respectively.

For the fair set of STARE, the approaches carry out noticeably sensitivity degradation against CTM by 10.19, 7.75, and 7.75 for SSVT, SSVVPPA, and SSHA, respectively but bring the slight absolute improvement against SS by 4.45, 6.89, and 6.89, respectively. For the poor sets, our proposed approaches improve sensitivity slightly on SS and report the absolute improvement in average by 2.49, 4.64, and 4.66, for SSVT, SSVVPPA, and SSHA, respectively.

For PPV, the performances of our proposed methods compared against CTM and SS are as follows. For the fair set of ROP, the absolute improvements of SSVT, SSVVPPA, and SSHA over CTM are all equal to 20.99 and over SS are also equal to 1.33. While the poor set reports the absolute improvement of SSVT, SSVVPPA, and SSHA against CTM significantly by 37.46, 28.32, 37.46, respectively and against SS by 30.84, 21.7, and 30.84, respectively.

For STARE collection, SSVT, SSVVPPA, and SSHA turn out the PPV degradation against CTM in fair set by 10.52, 8.54, and 8.54, respectively and yield the absolute improvement against SS by 7.05, 9.03, and 9.03, respectively. In poor collection, our proposed approaches improve PPV over both CTM and SS considerably. The improvements over CTM are 4.7, 2.5, 4.5, and over SS are 15.41, 13.21, 15.21, respectively for SSVT, SSVVPPA, and SSHA.

Furthermore, the general performance of average sensitivity for both collections delineates SSVT that produces the largest absolute improvement on a small scale by 1.91 and 2.06 against CTM and SS respectively whereas SSHA returns the highest absolute improvement of average PPV against CTM and SS substantially by 13.6 and 14.1, respectively.

Alternatively, SSVVPPA and SSHA approaches show the largest absolute improvement in the general performance of average sensitivity and PPV for the fair set of both collections by 0.21 and 6.22 against CTM and 4.48 and 5.18 against SS, respectively. For the poor set of both collections, SSHA is reported to show the

largest average sensitivity by absolute improvement 1.80 and 8.66 against CTM and SS respectively while SSVT yields the greatest average PPV in 21.08 of the absolute improvement against CTM and SSHA produces the maximum average PPA considerably by absolute improvement 23.03 against SS.

Generally the proposed approaches outperform SS and CTM regardless of the quality of the images and for each collection of data. In particular, when the image quality is poor, the proposed approaches outperform the other two approaches in terms of PPV considerably.

It should be noted that in [68] SS was found to be superior with regard to the OD segmentations based on the morphological operations [38] and the Circular Hough Transform applied to ROP [40]. Moreover, in [44] Lu has been claimed to outperform methods [48][49][50][75]. Therefore, the proposed approaches outperform the above-mentioned methods as well with a greater advantage.

It is worth noting that the SSHA is the integration on improvement among our proposed approaches (VVPPA and VT) to produce the optimal accuracy. The average absolute improvement on all collection by SSVT, SSVVPPA, and SSHA against CTM is respectively 1.93, 0.3, and 1.00 for the sensitivity and 13.16, 10.82, and 13.6 for the PPV. In addition, the average absolute improvement on all collection by SSVT, SSVVPPA, and SSHA against SS is respectively 2.06, 0.45, and 1.15 for the sensitivity and 13.66, 11.32, and 14.1 for the PPV.

Although CTM is claimed to be the fastest, its performance sturdily requires the optimum threshold on the gray level to select possible candidates for the center of the OD and the number of radial segments used to verify the circularity of the object boundary. Lu also claimed that the OD center nearly always lies within the first 20% brightest pixels within the probability map of the OD. However, there are a number of pathology images for which it is not always correct. In turn, the more this threshold is increased, the more computational time is produced. For instance, changing the percentage of the brightest pixel threshold from 20 to 60% double it. In addition, changing the angular step between the required radial segments from 6° to 2° increase

the computational time of CTM by a factor of 10. Our methods have been programmed in MATLAB and require in average about 3 minutes processing a standard database image 600x750 on a Dell computer with 3.30 GHz Intel Core i3 Processor and 4GB of random access memory. Table 7.3 shows the computational time in average of SSVT, SSVVPPA, and SSHA against CTM.

Table 7.3: The computational time CTM vs. our proposed approaches

Percentage of test pixels (%)	No. of radial line segments	Average time: CTM (mins)	Average Time (mins)		
			SSVT	SSVVPPA	SSHA
20	40	1.57	4.85	2.55	2.85
20	180	6.63			
60	40	4.29			
60	180	18.84			

Furthermore, the HA processes faster than the VT approach approximately twice, which is about 2 minutes for each image.

7.3 Discussions

In this section, we explain the cases that our proposed methods do not work.

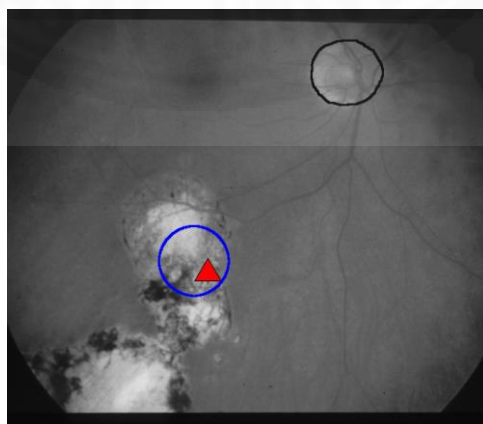


Figure 7.3: Inconclusive cases by VT (red triangle) and SSVT (blue circle) approaches

There are images where VT and SSVT fail as illustrated in Figure 7.3 and Figure 7.5 (right). Those images are usually characterized by unclear vascular networks or with noise and shadows of which its shape is similar to the vessels.

Figure 7.4 illustrates two failure cases of OD detection and segmentation using respectively the VVPPA and the SSVVPPA approaches. Even though the vessel network is distinguishable partially, there is a part of the image with uneven contrast between vessels and surroundings. As shown in Figure 7.4 (left), the extracted vessels are formed asymmetric structure. On the other hand, non-uniform illumination (bright refraction along retina edges) and the wider area of small lesions presence in Figure 7.4 (right) can sensitively affect vessel segmentation resulting the false OD segmentation.

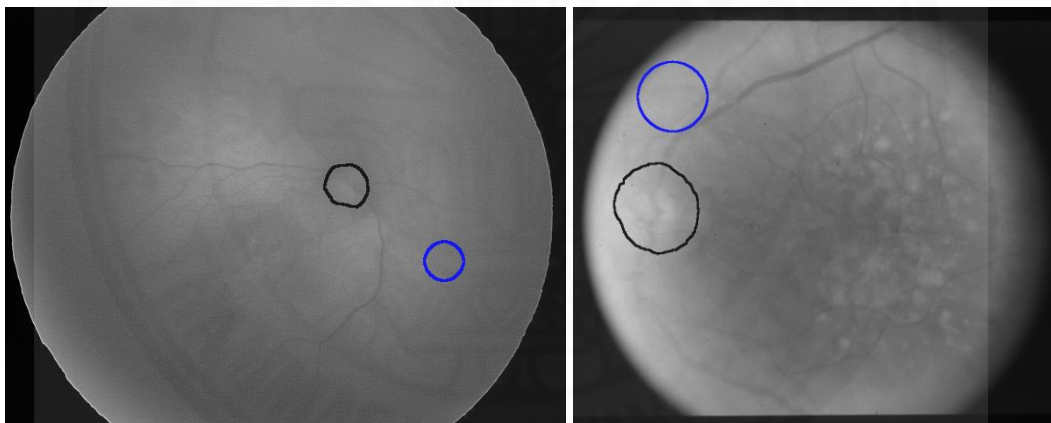


Figure 7.4: Inconclusive cases by SSVVPPA approach

As illustrated in Figure 7.5, two inconclusive cases in OD detection using the proposed approaches show the retinal images from poor collection in ROP and STARE. Retinal vessels are almost indistinguishable from background in Figure 7.5 (left) and the presence of vessel-like refraction, undesired illumination of too bright light, and deformed vessels are in Figure 7.5 (right) due to inadequate patient cooperation such as poor fixation or inability to stay still during the procedure. Even though, OD locating and detecting on these two cases can be success by CTM and SS.

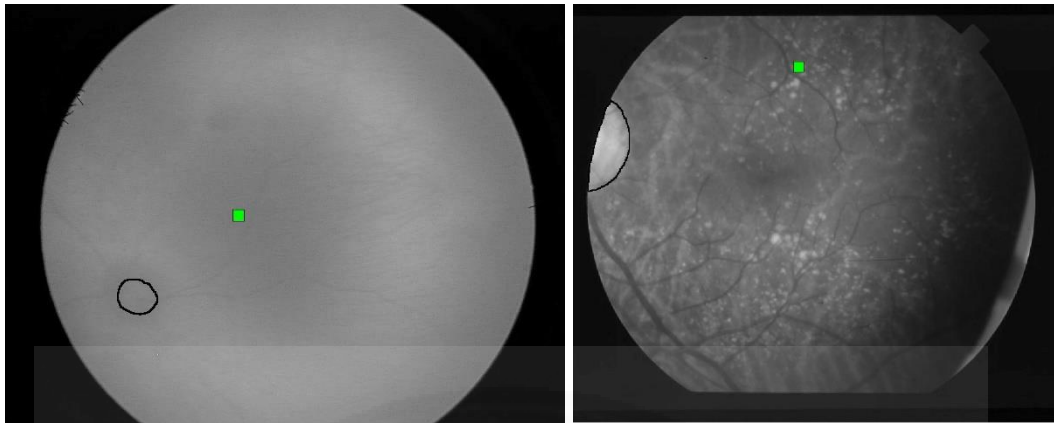
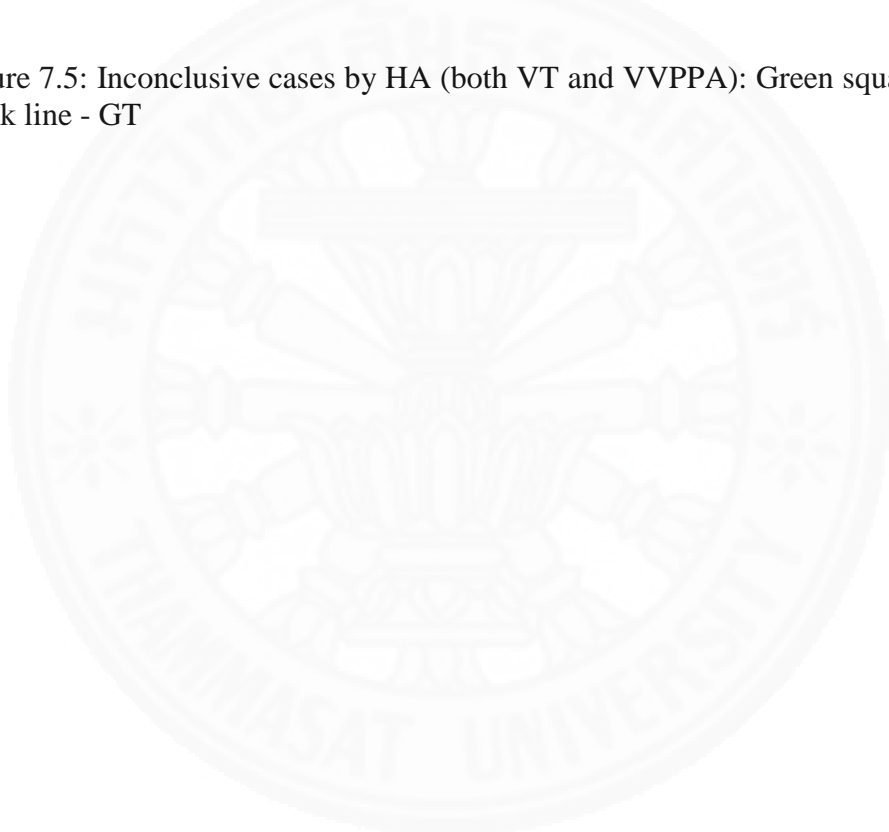


Figure 7.5: Inconclusive cases by HA (both VT and VVPPA): Green square - HA and black line - GT



Chapter 8

Conclusions and Recommendation for Future Work

In this chapter we summarize the main findings of our research, and recommend some areas for future work in section 8.1 and 8.2, respectively. Finally, in section 8.3 we discuss some other perspectives relating to this dissertation.

8.1 Thesis Summary

A number of automatic optic disk (OD) detection techniques have been proposed and some of these techniques reported a success rate of up to one hundred percent. Most OD detection techniques rely on features such as the size, shape, brightness, grey level, and contrast level of the OD. Such techniques generally only perform well with good quality images, showing a clear OD which is free from pathological abnormalities. However, they often fail to localize the OD in images of retinas with pathological features or in images of poor quality in which some of the expected features of the OD are absent. Due to the fact that the OD is the convergence points of the vessel networks and the vessel networks are usually present and traceable to localize the OD even in poor quality retinal images, we propose three methods for automatic OD localization and segmentation in retinal images based on the retinal vascular networks.

To localize the OD, three novel approaches have been proposed; the so-called *Vessel Transform* (VT), *Vessel Vector based Phase Portrait Analysis* (VVPPA), and *Hybrid Approach* (HA). VT approximates the location of the OD by finding the centroid of a collection of points of which the total sum of the distances from each point in this collection to all vessel clusters is minimum. VVPPA overcomes the OD localization problem by exploiting the fact that branch vessels are typically thinner and of low contrast than the main vessels, forming acute angles to the main vessels that typically lead to the center of the OD. To get the OD, the vessels are represented with vectors. The directions of vectors are determined based on the vessel features: the opposite angle, thickness, and contrast. Vectors adopted from the Mahfouz's approach for localization of the OD and the synthesized bouncing vectors which are specially

created to ensure the inside convergence are also included in the base vessel vectors to enhance the performance. These vectors are used to interpolate vectors at the grid points in the image. The region where these interpolated vectors converge is assumed to be the location of the OD. To analyze the convergence region, Phase Portrait Analysis is formulated. The HA selects when to use VT or VVPPA based on a set of image features, which are used to train a decision tree.

To obtain the OD boundary, our VT, VVPPA, and Hybrid methods are integrated with the OD segmentation algorithm proposed by Duangate et al. [68] based on SS. The integration generates three new segmentation methods namely SSVT, SSVVPPA, SSHA. The numerical VT and PPA scores contained from the VT and VVPPA, respectively, are used as additional features in the OD selection process of the SS [68]. To manipulate OD segmentation for our HA, either SSVT or SSVVPPA is selected according to the VT and VVPPA localization algorithms resulting from the hybrid algorithm.

We have tested the proposed approaches on two retinal fundus image databases: public (STARE) and local (ROP). There are a total of one hundred seventy-two images for these databases. Each database is divided into two sets by image quality, fair and poor, to test the performance of the algorithm in each group. We have demonstrated that all proposed OD localization methods considerably outperform the existing methods in terms of average accuracy across the whole collection of images. When comparing only the proposed approaches, the HA yields the highest results with 100% accuracy for the fair set of both databases, and 97.38 % for the poor set.

For the segmentation algorithms, we evaluated the performance using Positive Predictive value (PPV) and sensitivity. The baseline methods we used as a comparison are CTM [44] and SS [68]. Results show that generally our proposed approaches' performances are satisfactorily comparable to the base line methods. Specifically, the proposed approaches considerably outperform the baseline methods for the poor sets of images, and show slightly improved performance on the fair set. Among the proposed methods, SSVVPPA and SSHA yield the highest PPV and sensitivity. SSHA and SSVVPPA achieve the same values of 81.76% for PPV and

73.65% for sensitivity on the fair set of images. SSVT obtains the highest PPV of 79.12% while HA obtains the highest sensitivity of 53.05% for the poor set of images.

Precise OD identification is essential for computer-assisted diagnosis from retinal fundus images. The OD is a crucial component of the retina that can itself be used to detect many abnormalities in the eye, as well as being a key reference point for many other components in the retinal image analysis. The state-of-art results obtained in this work shows the wide applicability of our proposed techniques, which enable improved OD detection and segmentation accuracies in both fair and poor quality images. These findings can be used to improve computer-aided diagnosis in the field of ophthalmology, particularly when dealing with images of poor quality.

8.2 Recommendation for Future work

The following areas are proposed for future work, building on the successes demonstrated in this project.

- Instead of SS, another effective segmentation method such as circular transform by Lu et al. [44], watershed algorithm by Welfer et al. [75], or GVF snake [35] could be adapted to trace the OD contour.
- Applying a nature-inspired optimization algorithm such as particle swarm optimization or the firefly algorithms to trace randomly along blood vessels until they converge in the OD may also improve performance further.

8.3 Other perspectives

The methods proposed in this work still leave some gaps behind that could be mentioned on other perspectives as following.

- As an alternative to leading vector construction from a bifurcation, the vectors can be formulated differently to enhance the performance. Figure 8.1 shows another ways to turn vessels into vectors.

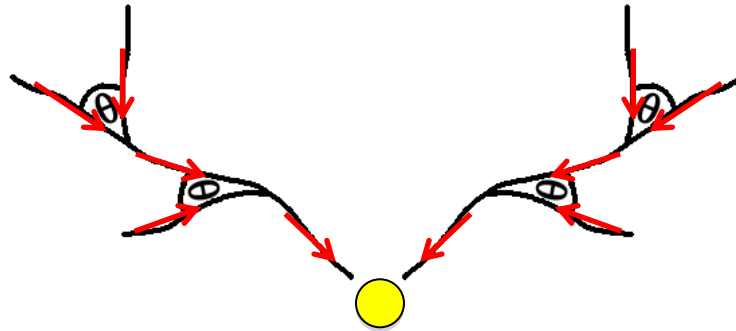


Figure 8.1: Illustration of an alternative way to construct vectors

The alternative vector construction could consider to construct three vectors pointing to the corresponding junction. A vector which is found the smallest opposite angle would be pointed outward from the corresponding junction. This concept could strengthen vector flow patterns in particular convergence pattern configuration.

- Further optimization of our methods is still required to improve running times.
- Our proposed approaches have thus far only been tested on retinal fundus images with a 35 and 45 degree field of view. Validating these results on larger images with a greater field of view would further enhance their utility.
- Finally, integrating unsupervised techniques, such as a genetic algorithm, for determining the optimum parameters for our methods for a given dataset would also make them more generally applicable to new unseen databases.

References

- [1] C. B. Estopinal, S. Ausayakhun, C. Jirawison, T. P. Margolis, and J. D. Keenan, "Access to Ophthalmologists in Thailand: A District-level Analysis," *Invest. Ophthalmol. Vis. Sci.*, vol. 53, no. 14, pp. 1422–1422, Mar. 2012.
- [2] C. B. Estopinal et al., "Access to ophthalmologic care in Thailand: a regional analysis," *Ophthalmic Epidemiol.*, vol. 20, no. 5, pp. 267–273, Oct. 2013.
- [3] Chaicharn Deerochanawong and Alessandra Ferrario, "Diabetes management in Thailand: a literature review of the burden, costs, and outcomes," *Deerochanawong Ferrario Glob. Health*, vol. 9, no. 11, pp. 1–18, 2013.
- [4] A. Hoover and M. Goldbaum, "Locating the optic nerve in a retinal image using the fuzzy convergence of the blood vessels," *IEEE Trans. Med. Imaging*, vol. 22, no. 8, pp. 951–958, Aug. 2003.
- [5] H. Li and O. Chutatape, "Automated feature extraction in color retinal images by a model based approach," *IEEE Trans. Biomed. Eng.*, vol. 51, no. 2, pp. 246–254, Feb. 2004.
- [6] R. R. A. Bourne et al., "Prevalence of glaucoma in Thailand: a population based survey in Rom Klao District, Bangkok," *Br. J. Ophthalmol.*, vol. 87, no. 9, pp. 1069–1074, Sep. 2003.
- [7] B. J. Zitelli, S. C. McIntire, and A. J. Nowalk, *Zitelli and Davis' Atlas of Pediatric Physical Diagnosis: Expert Consult - Online*. Elsevier Health Sciences, 2012.
- [8] J. B. Selhorst and Y. Chen, "The optic nerve," *Semin. Neurol.*, vol. 29, no. 1, pp. 29–35, Feb. 2009.
- [9] E. G. Dallas, R. A. Clement, and D. S. I. Taylor, "Diagnosis from fundus photographs," *Br. J. Ophthalmol.*, vol. 91, no. 5, pp. 608–612, May 2007.
- [10] M. Lalonde, M. Beaulieu, and L. Gagnon, "Fast and robust optic disc detection using pyramidal decomposition and Hausdorff-based template matching," *IEEE Trans. Med. Imaging*, vol. 20, no. 11, pp. 1193–1200, Nov. 2001.

- [11] H. F. Jelinek, C. Depardieu, C. Lucas, D. J. Cornforth, W. Huang, and M. J. Cree, "Towards vessel characterization in the vicinity of the optic disc in digital retinal images," in *Image Vis Comput Conf*, 2005, pp. 2–7.
- [12] M. Niemeijer, M. D. Abramoff, and B. van Ginneken, "Fast detection of the optic disc and fovea in color fundus photographs," *Med. Image Anal.*, vol. 13, no. 6, pp. 859–870, Dec. 2009.
- [13] A. Dehghani, H. A. Moghaddam, and M.-S. Moin, "Optic disc localization in retinal images using histogram matching," *EURASIP J. Image Video Process.*, vol. 2012, no. 1, pp. 1–11, Oct. 2012.
- [14] M. J. Cox and I. C. J. Wood, "Computer-assisted optic nerve head assessment," *Ophthalmic Physiol. Opt.*, vol. 11, no. 1, pp. 27–35, Jan. 1991.
- [15] M. J. C. D. T. Morris, "Automated Extraction Of The Optic Nerve Head Rim.," In: *American Academy of Optometry Annual Conference; 1993.*, 01-Dec-1993. [Online]. Available: <https://www.escholar.manchester.ac.uk/uk-ac-man-scw:2a722>. [Accessed: 24-Jun-2016].
- [16] R. J. Winder, P. J. Morrow, I. N. McRitchie, J. R. Bailie, and P. M. Hart, "Algorithms for digital image processing in diabetic retinopathy," *Comput. Med. Imaging Graph.*, vol. 33, no. 8, pp. 608–622, Dec. 2009.
- [17] Brady M. and Lee S., "Visual monitoring of glaucoma," *Image Vis. Comput.*, vol. 9, no. 4, pp. 39–44, 1991.
- [18] J. Xu, O. Chutatape, and P. Chew, "Automated Optic Disk Boundary Detection by Modified Active Contour Model," *IEEE Trans. Biomed. Eng.*, vol. 54, no. 3, pp. 473–482, Mar. 2007.
- [19] C. Wang, D. Kaba, and Y. Li, "Level Set Segmentation of Optic Discs from Retinal Images," *J. Med. Bioeng. Vol.*, vol. 4, no. 3, 2015.
- [20] V. Thongnuch and B. Uyyanonvara, "Automatic optic disk detection from low contrast retinal images of ROP infant using GVF snake," *Suranaree J Sci Technol*, vol. 14, no. 3, pp. 223–34, 2007.
- [21] H. Li and O. Chutatape, "A model-based approach for automated feature extraction in fundus images," in *Ninth IEEE International Conference on Computer Vision, 2003. Proceedings, 2003*, pp. 394–399 vol.1.

- [22] H. Li and O. Chutatape, "Boundary detection of optic disk by a modified ASM method," *Pattern Recognit.*, vol. 36, no. 9, pp. 2093–2104, Sep. 2003.
- [23] J. Lowell et al., "Optic nerve head segmentation," *IEEE Trans. Med. Imaging*, vol. 23, no. 2, pp. 256–264, Feb. 2004.
- [24] U. M. Akram and S. A. Khan, "Automated Detection of Dark and Bright Lesions in Retinal Images for Early Detection of Diabetic Retinopathy," *J. Med. Syst.*, vol. 36, no. 5, pp. 3151–3162, Nov. 2011.
- [25] M. Blanco, M. G. Penedo, N. Barreira, M. Penas, and M. J. Carreira, "Localization and Extraction of the Optic Disc Using the Fuzzy Circular Hough Transform," in *Artificial Intelligence and Soft Computing – ICAISC 2006*, L. Rutkowski, R. Tadeusiewicz, L. A. Zadeh, and J. M. Żurada, Eds. Springer Berlin Heidelberg, 2006, pp. 712–721.
- [26] A. Aquino, M. E. Gegundez, and D. Marin, "Automated optic disc detection in retinal images of patients with diabetic retinopathy and risk of macular edema," *Int. J. Biol. Life Sci.*, vol. 8, no. 2, pp. 87–92, 2012.
- [27] C. Sinthanayothin, J. F. Boyce, H. L. Cook, and T. H. Williamson, "Automated localisation of the optic disc, fovea, and retinal blood vessels from digital colour fundus images," *Br. J. Ophthalmol.*, vol. 83, no. 8, pp. 902–910, Aug. 1999.
- [28] M. Esmaeili, H. Rabbani, A. M. Dehnavi, and A. Dehghani, "Automatic detection of exudates and optic disk in retinal images using curvelet transform," *IET Image Process.*, vol. 6, no. 7, pp. 1005–1013, Oct. 2012.
- [29] M. Esmaeili, H. Rabbani, and A. M. Dehnavi, "Automatic optic disk boundary extraction by the use of curvelet transform and deformable variational level set model," *Pattern Recognit.*, vol. 45, no. 7, pp. 2832–2842, Jul. 2012.
- [30] S. Shahbeig and H. Pourghassem, "Fast and automatic algorithm for optic disc extraction in retinal images using principle-component-analysis-based preprocessing and curvelet transform," *J. Opt. Soc. Am. A*, vol. 30, no. 1, p. 13, Jan. 2013.
- [31] C. Pereira, L. Gonçalves, and M. Ferreira, "Optic disc detection in color fundus images using ant colony optimization," *Med. Biol. Eng. Comput.*, vol. 51, no. 3, pp. 295–303, Nov. 2012.

- [32] S. Morales, V. Naranjo, J. Angulo, and M. Alcañiz, "Automatic Detection of Optic Disc Based on PCA and Mathematical Morphology," *IEEE Trans. Med. Imaging*, vol. 32, no. 4, pp. 786–796, Apr. 2013.
- [33] H.-K. Hsiao, C.-C. Liu, C.-Y. Yu, S.-W. Kuo, and S.-S. Yu, "A novel optic disc detection scheme on retinal images," *Expert Syst. Appl.*, vol. 39, no. 12, pp. 10600–10606, Sep. 2012.
- [34] S. A. Ramakanth and R. V. Babu, "Approximate Nearest Neighbour Field based Optic Disk Detection," *Comput. Med. Imaging Graph.*, vol. 38, no. 1, pp. 49–56, Jan. 2014.
- [35] A. Giachetti, L. Ballerini, and E. Trucco, "Accurate and reliable segmentation of the optic disc in digital fundus images," *J. Med. Imaging*, vol. 1, no. 2, pp. 024001–024001, 2014.
- [36] D. Kavitha and S. S. Devi, "Automatic detection of optic disc and exudates in retinal images," in *Proceedings of 2005 International Conference on Intelligent Sensing and Information Processing, 2005.*, 2005, pp. 501–506.
- [37] J. Tobin Kenneth W., E. Chaum, V. P. Govindasamy, T. P. Karnowski, and O. Sezer, "Characterization of the optic disc in retinal imagery using a probabilistic approach," 2006, vol. 6144, p. 61443F–61443F–10.
- [38] A. Sopharak, B. Uyyanonvara, S. Barman, and T. H. Williamson, "Automatic detection of diabetic retinopathy exudates from non-dilated retinal images using mathematical morphology methods," *Comput. Med. Imaging Graph.*, vol. 32, no. 8, pp. 720–727, Dec. 2008.
- [39] T. F. Cootes, C. J. Taylor, D. H. Cooper, and J. Graham, "Active Shape Models-Their Training and Application," *Comput. Vis. Image Underst.*, vol. 61, no. 1, pp. 38–59, Jan. 1995.
- [40] S. Sekhar, W. Al-Nuaimy, and A. K. Nandi, "Automated localisation of retinal optic disk using Hough transform," in *2008 5th IEEE International Symposium on Biomedical Imaging: From Nano to Macro, 2008*, pp. 1577–1580.
- [41] X. Zhu and R. M. Rangayyan, "Detection of the optic disc in images of the retina using the Hough transform," in *2008 30th Annual International*

- Conference of the IEEE Engineering in Medicine and Biology Society, 2008, pp. 3546–3549.
- [42] A. Azuara-Blanco, A. Harris, L. B. Cantor, M. M. Abreu, and M. Weinland, “Effects of short term increase of intraocular pressure on optic disc cupping,” *Br. J. Ophthalmol.*, vol. 82, no. 8, pp. 880–883, Aug. 1998.
- [43] A. V. Sagar, S. Balasubramanian, and V. Chandrasekaran, “Automatic Detection of Anatomical Structures in Digital Fundus Retinal Images.,” in *MVA*, 2007, pp. 483–486.
- [44] S. Lu, “Accurate and Efficient Optic Disc Detection and Segmentation by a Circular Transformation,” *IEEE Trans. Med. Imaging*, vol. 30, no. 12, pp. 2126–2133, Dec. 2011.
- [45] D. Welfer, J. Scharcanski, C. M. Kitamura, M. M. Dal Pizzol, L. W. B. Ludwig, and D. R. Marinho, “Segmentation of the optic disk in color eye fundus images using an adaptive morphological approach,” *Comput. Biol. Med.*, vol. 40, no. 2, pp. 124–137, Feb. 2010.
- [46] A. A. H. A. R. Youssif, A. Z. Ghalwash, and A. A. S. A. R. Ghoneim, “Optic Disc Detection From Normalized Digital Fundus Images by Means of a Vessels’ Direction Matched Filter,” *IEEE Trans. Med. Imaging*, vol. 27, no. 1, pp. 11–18, Jan. 2008.
- [47] A. E. Mahfouz and A. S. Fahmy, “Ultrafast Localization of the Optic Disc Using Dimensionality Reduction of the Search Space,” in *Medical Image Computing and Computer-Assisted Intervention – MICCAI 2009*, G.-Z. Yang, D. Hawkes, D. Rueckert, A. Noble, and C. Taylor, Eds. Springer Berlin Heidelberg, 2009, pp. 985–992.
- [48] E. J. Carmona, M. Rincón, J. García-Feijóo, and J. M. Martínez-de-la-Casa, “Identification of the optic nerve head with genetic algorithms,” *Artif. Intell. Med.*, vol. 43, no. 3, pp. 243–259, Jul. 2008.
- [49] M. Foracchia, E. Grisan, and A. Ruggeri, “Detection of optic disc in retinal images by means of a geometrical model of vessel structure,” *IEEE Trans. Med. Imaging*, vol. 23, no. 10, pp. 1189–1195, Oct. 2004.
- [50] S. Ravishankar, A. Jain, and A. Mittal, “Automated feature extraction for early detection of diabetic retinopathy in fundus images,” in *IEEE Conference on*

- Computer Vision and Pattern Recognition, 2009. CVPR 2009, 2009, pp. 210–217.
- [51] K. Akita and H. Kuga, “A computer method of understanding ocular fundus images,” *Pattern Recognit.*, vol. 15, no. 6, pp. 431–443, Jan. 1982.
- [52] R. Chrastek et al., “Multimodal retinal image registration for optic disk segmentation,” *Methods Inf. Med.*, vol. 43, no. 4, pp. 336–342, 2004.
- [53] A. Dehghani, M.-S. Moin, and M. Saghafi, “Localization of the optic disc center in retinal images based on the Harris corner detector,” *Biomed. Eng. Lett.*, vol. 2, no. 3, pp. 198–206, Oct. 2012.
- [54] D. Zhang and Y. Zhao, “Novel Accurate and Fast Optic Disc Detection in Retinal Images With Vessel Distribution and Directional Characteristics,” *IEEE J. Biomed. Health Inform.*, vol. 20, no. 1, pp. 333–342, Jan. 2016.
- [55] A. M. Mendonça, A. Sousa, L. Mendonça, and A. Campilho, “Automatic localization of the optic disc by combining vascular and intensity information,” *Comput. Med. Imaging Graph.*, vol. 37, no. 5–6, pp. 409–417, Jul. 2013.
- [56] B. Dashtbozorg, A. M. Mendonça, and A. Campilho, “Optic disc segmentation using the sliding band filter,” *Comput. Biol. Med.*, vol. 56, pp. 1–12, Jan. 2015.
- [57] J. Xu, O. Chutatape, E. Sung, C. Zheng, and P. Chew Tec Kuan, “Optic disk feature extraction via modified deformable model technique for glaucoma analysis,” *Pattern Recognit.*, vol. 40, no. 7, pp. 2063–2076, Jul. 2007.
- [58] A. S. Semashko, A. S. Krylov, and A. S. Rodin, “Using Blood Vessels Location Information in Optic Disk Segmentation,” in *Image Analysis and Processing – ICIAP 2011*, G. Maino and G. L. Foresti, Eds. Springer Berlin Heidelberg, 2011, pp. 384–393.
- [59] S. Chaudhuri, S. Chatterjee, N. Katz, M. Nelson, and M. Goldbaum, “Automatic detection of the optic nerve in retinal images,” in *IEEE International Conference on Image Processing*, 1989, pp. 1–5.
- [60] A. Hoover and M. Goldbaum, “Fuzzy convergence,” in *1998 IEEE Computer Society Conference on Computer Vision and Pattern Recognition*, 1998. Proceedings, 1998, pp. 716–721.

- [61] R. M. Rangayyan, X. Zhu, F. J. Ayres, and A. L. Ells, "Detection of the Optic Nerve Head in Fundus Images of the Retina with Gabor Filters and Phase Portrait Analysis," *J. Digit. Imaging*, vol. 23, no. 4, pp. 438–453, Jan. 2010.
- [62] S. Chucherd, A. Rodtook, and S. S. Makhanov, "Phase Portrait Analysis for Multiresolution Generalized Gradient Vector Flow," *IEICE Trans. Inf. Syst.*, vol. E93–D, no. 10, pp. 2822–2835, Oct. 2010.
- [63] S. Chucherd and S. S. Makhanov, "Sparse phase portrait analysis for preprocessing and segmentation of ultrasound images of breast Cancer," *IAENG Int. J. Comput. Sci.*, vol. 38, no. 2, pp. 146–159, 2011.
- [64] D. W. Jordan and P. Smith, *Nonlinear Ordinary Differential Equations: An Introduction to Dynamical Systems*. Oxford University Press, 1999.
- [65] S. Chucherd and S. S. Makhanov, "Multiresolution phase portrait analysis for segmentation of ultrasound images for detection of breast cancer," in *Proceedings of the International MultiConference of Engineers and Computer Scientists*, 2011, vol. 1.
- [66] A. Witkin, "Scale-space filtering: A new approach to multi-scale description," in *Acoustics, Speech, and Signal Processing, IEEE International Conference on ICASSP '84.*, 1984, vol. 9, pp. 150–153.
- [67] T. Lindeberg, *Scale-Space Theory in Computer Vision*. Springer Science & Business Media, 2013.
- [68] C. Duanggate, B. Uyyanonvara, S. S. Makhanov, S. Barman, and T. Williamson, "Parameter-free optic disc detection," *Comput. Med. Imaging Graph.*, vol. 35, no. 1, pp. 51–63, Jan. 2011.
- [69] L. Sukkaew, B. Uyyanonvara, S. Barman, A. Fielder, and K. Cocker, "Automatic extraction of the structure of the retinal blood vessel network of premature infants," *J. Med. Assoc. Thail. Chotmaihet Thangphaet*, vol. 90, no. 9, pp. 1780–1792, Sep. 2007.
- [70] U. T. V. Nguyen, A. Bhuiyan, L. A. F. Park, and K. Ramamohanarao, "An effective retinal blood vessel segmentation method using multi-scale line detection," *Pattern Recognit.*, vol. 46, no. 3, pp. 703–715, Mar. 2013.

- [71] S. Badsha, A. W. Reza, K. G. Tan, and K. Dimyati, "A New Blood Vessel Extraction Technique Using Edge Enhancement and Object Classification," *J. Digit. Imaging*, vol. 26, no. 6, pp. 1107–1115, Mar. 2013.
- [72] Hoover, A and Goldbaum, M., "The STructure Analysis of the RETina (STARE) project." .
- [73] P. Bankhead, C. N. Scholfield, J. G. McGeown, and T. M. Curtis, "Fast Retinal Vessel Detection and Measurement Using Wavelets and Edge Location Refinement," *PLOS ONE*, vol. 7, no. 3, p. e32435, Mar. 2012.
- [74] P. Bankhead, "ARIA: Retinal vessel detection using MATLAB." Belfast, UK, 2011.
- [75] D. Welfer, J. Scharcanski, and D. R. Marinho, "A morphologic two-stage approach for automated optic disk detection in color eye fundus images," *Pattern Recognit. Lett.*, vol. 34, no. 5, pp. 476–485, Apr. 2013.

Appendix A

List of Publications

International Journals

1. Muangnak, N., Aimmanee, P., Makhanov, SS., Uyyanonvara, B. (2015). Vessel transform for automatic optic disk detection in retinal images. *IET Image Processing*. 9(9), 743-750.

International Conferences

1. Muangnak, N., Aimmanee, P., Makhanov, SS., Uyyanonvara, B. (2012, March). *An improve optic disc detection on low quality retinal images with entropy thresholding*. Paper presented at the Third International Conference on Information and Communication Technology for Embedded Systems.
2. Bornschlegel, T., Muangnak, N., Aimmanee, P., Makhanov, SS., Uyyanonvara, B. (2012, December). *Finding curves's convergence using delaunay search*. Paper presented at the First Asian Conference on Information Systems, ACIS 2012, At Siem Reap, Cambodia.
3. Tangseng, P., Muangnak, N., Aimmanee, P., Makhanov, SS., Uyyanonvara, B. (2013, October). *A study of retinal blood vessel clustering for finding the main vessel convergence*. Paper presented at the Second Asian Conference on Information Systems, ACIS 2013, Phuket, Thailand.
4. Prukpaiboon, N., Chotvijit, S., Muangnak, N., Aimmanee, P. (2013, October). *Comparative study of initial seed point required approaches with the use of vessel distance hint for OD boundary detection*. Paper presented at the Second Asian Conference on Information Systems, ACIS 2013, Phuket, Thailand.